JOURNAL OF GUIDANCE, CONTROL, AND DYNAMICS
Vol. 41, No. 6, June 2018

Minimum-Effort Intercept Angle Guidance with Multiple-Obstacle Avoidance

Shashi Ranjan Kumar*
Indian Institute of Technology Bombay, Powai, Mumbai 400 076, India
and
Martin Weiss† and Tal Shima‡
Technion–Israel Institute of Technology, 32000 Haifa, Israel

DOI: 10.2514/1.G003223

This paper presents an intercept angle guidance law against moving targets in an environment with several static obstacles. The guidance law is derived based on linearized kinematics model. By minimizing the guidance effort subjected to the conditions where the target is intercepted at the specified impact angle and the obstacles are avoided by specified minimum distances, the basic guidance algorithm is obtained. The special cases of one and two obstacles are separately considered. The proposed guidance law has a form similar to that of augmented proportional navigation guidance with some additional bias terms. These bias terms correspond to the correction for the impact angle error and the generation of the required maneuvers to avoid the obstacles. Finally, numerical simulations are used to illustrate the efficacy of the proposed guidance law.

I. Introduction

THE ability of a guidance law to enforce an impact angle may increase the effectiveness of an interceptor, reduce the warhead size, and consequently reduce the collateral damage. In many applications, the guidance law also needs to ensure a minimum distance of the missile from obstacles along its trajectory in addition to satisfying the terminal constraints. Such situations may arise in practical scenarios where a missile has to intercept the target while avoiding collision with some friendly or neutral structures.

One of the early attempts to design guidance laws for controlling interception angle was made in [1], where Kim and Grider used a linear quadratic optimal control formulation under the assumption of a nonmaneuvering target and a negligible angle of attack. Later, in [2,3], guidance laws were also derived as the solution of a linear optimal control problem subjected to various performance criteria, such as minimization of a weighted control effort. Guidance laws in [1–3] were derived using the linearized engagement dynamics. In [4], a three-dimensional adaptive guidance approach for a hypersonic gliding vehicle in proportional navigation (PN) form was proposed for imposing the impact angle criterion. To ensure higher precision in the impact angle conditions, the initial selection of the guidance parameters and its closed-loop and nonlinear adaptation laws were suggested. In [5], a proportional-navigation-based impact angle guidance law was proposed that took look angle and acceleration bounds into account. The PN guidance gain was determined by solving an optimal control problem as a sequence of convex optimization problems at every guidance cycle. In [6,7], guidance laws were proposed to impose impact angle constraints using variants of the PN guidance strategy. A guidance law proposed in [8] ensured interception at a desired impact angle by following a circular arc to the target. In [9], a guidance concept to impose an impact angle was proposed using the principle of following a constant inscribed angle in a circle. Guidance laws based on the inscribed angle concept were proposed using linear [9,10] as well as nonlinear [11] engagement kinematics. Nonlinear control techniques, such as sliding-mode control, were also used for designing impact angle constrained guidance laws [12–15].

All the guidance laws presented in [1–15] enabled the interceptor to achieve desired impact angles. But, none of them addressed the possible presence of obstacles in the engagement scenarios. There exist three broad classes of methods for collision avoidance, represented by motion planning methods [16–21], geometric guidance approaches [22–26], and artificial potential field methods [27–30].

The first class contains diverse methods such as planning based on the rapidly exploring random trees (RRTs) algorithm [16,17], dynamic programming [18], deterministic graph search [19,20], and probabilistic graph search [21]. These methods work with arbitrarily complex vehicle dynamics. However, it is difficult to assess their performance due to their inherent complexity. These methods usually provide open-loop solutions that require regular updates to account for new data or modeling errors. Due to the intensive computational requirements, these methods may not be appropriate for missile guidance applications.

A second class of methods is based on geometric guidance approaches [22–26]. In [22], after detecting a possible collision with an obstacle, an aim point was selected on the boundary of the safety zone surrounding the obstacle. Finally, PN guidance was used to change the course of the vehicle to reach the chosen aim point, thus avoiding obstacles. Guidance laws based on the collision cone method [23,24] and the velocity obstacle method [25] also share a similar structure. In the same framework, a minimum-effort path to the aim point using optimization was proposed in [26]. In this class of methods, collision detection and collision avoidance are performed sequentially, which may result in performance degradation.

Another class of methods is based on artificial potential field methods [27–29]. The guidance command using this method is obtained by adding the field forces corresponding to the obstacles and the goal. Unlike the geometric guidance methods, the collision detection and collision avoidance are integrated in a single operation. The performance of these guidance laws [27–29] depends on the choice of the potential field function. Because the relation between the potential field function and the vehicle performance is not straightforward, it is difficult to optimize the performance of guidance law. However, this class of methods seems most appropriate for the missile guidance applications. In [30], a multimissile distributed guidance algorithm was proposed for achieving a salvo attack with obstacle avoidance. The guidance command consisted of

Received 31 July 2017; revision received 16 October 2017; accepted for publication 19 October 2017; published online 28 November 2017.

*Assistant Professor, Department of Aerospace Engineering; srk.technion@gmail.com.

†Research Scientist, Faculty of Aerospace Engineering; weissm@technion.ac.il.

‡Associate Professor, Faculty of Aerospace Engineering; tal.shima@technion.ac.il. Associate Fellow AIAA.

terms accounting for target interception, impact time error, and obstacle avoidance.

It is important to note that the guidance laws in [1–15] did not consider obstacle avoidance, and those in [17–30] did not take into account the impact angle constraints. The problem of imposing an intercept angle while avoiding obstacles has not received much attention in the missile guidance literature. However, such scenarios are of paramount importance from the perspective of real-world scenarios. In [16], an intercept angle guidance law for an obstacle-rich environment was derived using a variant of the RRTs algorithm.

In this paper, an intercept angle guidance law is proposed against a moving target. This guidance law enables the missile to achieve its objective even in the presence of several obstacles along the trajectory. First, a guidance law is derived for the general case with multiple obstacles using linearized engagement kinematics and optimal control theory. Later, the special cases of one and two obstacles in the engagement scenario are analyzed. Guidance laws for these cases take the form of augmented PN guidance with some additional bias terms. These bias terms correspond to the correction for impact angle error, the detection of obstacles, and subsequently the generation of required guidance commands to avoid the collision of missiles with them.

The organization of paper is as follows. In the next section, the nonlinear and linearized models of the engagement are presented and the guidance problem of interception while avoiding obstacles is formulated as an optimal control problem. Section III presents the derivation of the guidance laws. In Sec. IV, the performance of the proposed guidance laws is evaluated for different engagement scenarios. Finally, concluding remarks are given in Sec. V.

II. Problem Formulation

Consider a schematic view of the planar engagement scenario, shown in Fig. 1, where a missile is launched to intercept a target while avoiding multiple obstacles along the way. The missile and the target are assumed to be point mass vehicles.

A. Nonlinear Engagement Kinematics

In this section, the nonlinear kinematics for planar engagements will be presented. In Fig. 1, the coordinate frame $X_I O Y_I$ represents the Cartesian inertial coordinate system. The speed and lateral acceleration of both the missile and the target are denoted by the pairs (V_M, a_M) and (V_T, a_T), respectively. The distances from the missile to the target and the ith obstacle are denoted by r and r_{io}, respectively. Their corresponding line-of-sight (LOS) angles are denoted by λ and λ_{io}, respectively. The speeds of both the missile and the target are assumed to be constant throughout the engagement. The engagement kinematics between missile–target and missile–obstacle pairs are given by

$$\dot{r} = V_r = -[V_M \cos(\gamma_M - \lambda) + V_T \cos(\gamma_T + \lambda)] \tag{1a}$$

$$r\dot{\lambda} = V_\lambda = -V_M \sin(\gamma_M - \lambda) + V_T \sin(\gamma_T + \lambda) \tag{1b}$$

$$\dot{r}_{io} = V_{r_{io}} = -V_M \cos(\gamma_M - \lambda_{io}) \tag{1c}$$

$$r_{io}\dot{\lambda}_{io} = V_{\lambda_{io}} = -V_M \sin(\gamma_M - \lambda_{io}) \tag{1d}$$

for $i = 1, \ldots, N$, where N is the total number of obstacles. The flight-path angles of the missile and the target are governed by

$$\dot{\gamma}_M = \frac{a_M}{V_M}, \qquad \dot{\gamma}_T = \frac{a_T}{V_T} \tag{2}$$

The missile and the target are assumed to have ideal dynamics. The impact angle is defined as the angle between the velocity vectors of missile and target at interception, as shown in Fig. 1. Note that the impact angle is equal to the final value of variable $\gamma = \gamma_M + \gamma_T$ at the time of interception of the target.

B. Linearized Engagement Kinematics

In this section, the engagement kinematics are presented using a linear framework. In order to linearize the engagement model, it is assumed that the missile and the target have small deviations from their collision course, and that their flight-path and LOS angles are relatively small. It is also assumed that the obstacles are located near the collision course trajectory. The X axis of the coordinate frame XOY in Fig. 1 is assumed to be aligned with the initial missile–target LOS. In Fig. 1, the accelerations of the missile and target perpendicular to the initial target–missile LOS are denoted by a_{MN} and a_{TN}, respectively. Relative displacements of the target–missile and the ith obstacle–missile normal to the initial LOS, as shown in Fig. 1, are denoted by z and z_{io}, respectively. Lateral accelerations of the missile and the target normal to the initial LOS can be defined as

$$\begin{aligned} a_{MN} &= a_M \chi_{M_0}, \qquad a_{TN} = a_T \chi_{T_0}, \\ \chi_{M_0} &= \cos(\gamma_M - \lambda_0), \qquad \chi_{T_0} = \cos(\gamma_T + \lambda_0) \end{aligned} \tag{3}$$

where λ_0 is the initial LOS angle of missile–target engagement. The state vector of the missile–target–obstacle engagement is defined as

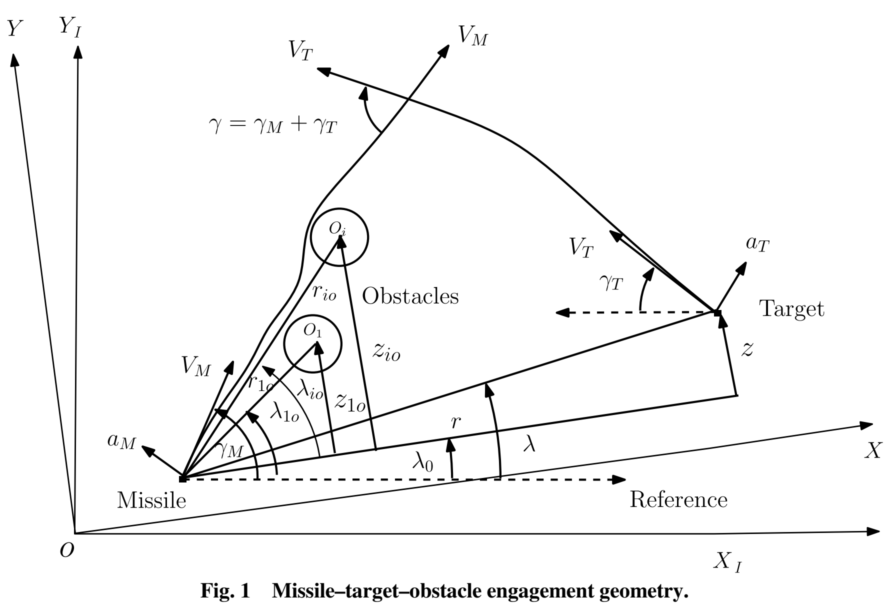

Fig. 1 Missile–target–obstacle engagement geometry.

$$\begin{aligned} \boldsymbol{x} &= [x_1 \quad x_2 \quad x_3 \quad x_4 \quad x_5 \quad \cdots \quad x_{2N+3}]^T \\ &= [z \quad \dot{z} \quad \gamma \quad z_{1o} \quad \dot{z}_{1o}, \quad \cdots \quad z_{io} \quad \dot{z}_{io}, \quad \cdots \quad z_{No} \quad \dot{z}_{No}]^T \end{aligned} \tag{4}$$

The equations of motion in this linearized framework can be written as

$$\begin{aligned} \dot{x}_1 &= x_2 \\ \dot{x}_2 &= a_{TN} - a_{MN} \\ \dot{x}_3 &= \frac{a_{TN}}{V_T'} + \frac{a_{MN}}{V_M'} \\ \dot{x}_{2i+2} &= x_{2i+3} \\ \dot{x}_{2i+3} &= -a_{MN}, \quad \forall i = 1, 2, \ldots, N \end{aligned} \tag{5}$$

where $V_T' = V_T \cos(\gamma_{T_0} + \lambda_0)$ and $V_M' = V_M \cos(\gamma_{M_0} - \lambda_0)$. In matrix form, the engagement dynamics can be written as

$$\dot{\boldsymbol{x}} = \boldsymbol{A}x + \boldsymbol{B}a_{MN} + \boldsymbol{C}a_{TN} \tag{6}$$

where

$$\boldsymbol{A} = \begin{bmatrix} \boldsymbol{A}_0 & [0] \\ [0] & \boldsymbol{A}_{ob} \end{bmatrix}, \quad \boldsymbol{B} = \begin{bmatrix} \boldsymbol{B}_0 \\ \boldsymbol{B}_{ob} \end{bmatrix}, \quad \boldsymbol{C} = \begin{bmatrix} \boldsymbol{C}_0 \\ [0] \end{bmatrix}$$

$$\boldsymbol{A}_0 = \begin{bmatrix} 0 & 1 & 0 \\ 0 & 0 & 0 \\ 0 & 0 & 0 \end{bmatrix}, \quad \boldsymbol{B}_0 = \begin{bmatrix} 0 \\ -1 \\ 1/V_M' \end{bmatrix}, \quad \boldsymbol{C}_0 = \begin{bmatrix} 0 \\ 1 \\ 1/V_T' \end{bmatrix}$$

$$\boldsymbol{A}_{ob} = \begin{bmatrix} \boldsymbol{A}_{1o} & \vdots & [0] & \vdots & [0] \\ \cdots & \cdots & \cdots & \cdots & \cdots \\ [0] & \vdots & \boldsymbol{A}_{io} & \vdots & [0] \\ \cdots & \cdots & \cdots & \cdots & \cdots \\ [0] & \vdots & [0] & \vdots & \boldsymbol{A}_{No} \end{bmatrix}, \quad \boldsymbol{B}_{ob} = \begin{bmatrix} \boldsymbol{B}_{1o} \\ \vdots \\ \boldsymbol{B}_{io} \\ \vdots \\ \boldsymbol{B}_{No} \end{bmatrix}$$

$$\boldsymbol{A}_{io} = \begin{bmatrix} 0 & 1 \\ 0 & 0 \end{bmatrix}, \quad \boldsymbol{B}_{io} = \begin{bmatrix} 0 \\ -1 \end{bmatrix}, \quad \forall i = 1, \ldots, N \tag{7}$$

where [0] represents a matrix with zeros of the appropriate dimensions.

The time-to-go (t_{go}) for missile–target and missile–obstacle engagements, under small angle assumptions, can be approximated by

$$t_{\mathrm{go}} = \frac{r}{-V_r} \tag{8a}$$

$$t_{\mathrm{go}_i} = \frac{r_{io}}{V_M}, \quad \forall i = 1, \ldots, N \tag{8b}$$

Without loss of generality, it is assumed here that the obstacles are numbered in such a way that the conditions $t_{\mathrm{go}_i} < t_{\mathrm{go}_{(i+1)}}$ $\forall i = 1, \ldots, (N-1)$ are always true. The differences between the time-to-go approximations are denoted as

$$\Delta_i = t_f - t_{f_i} = t_{\mathrm{go}} - t_{\mathrm{go}_i}, \quad \forall i = 1, \ldots, N \tag{9}$$

where t_f and t_{f_i} are the times taken by the missile to intercept the target and pass the ith obstacle, respectively. To minimize the total control effort, the cost function J_{cost} can be defined as

$$J_{\mathrm{cost}} = \int_0^{t_f} a_{MN}^2 \,\mathrm{d}t \tag{10}$$

Note that minimizing the control effort helps in reducing the drag acting on the missile.

For the problem statement, consider a planar engagement with a target that performs a constant maneuver. The problem is to find the missile lateral acceleration a_{MN} that minimizes the cost function given by Eq. (10), subjected to Eq. (5), while avoiding obstacles and intercepting a moving target at a desired impact angle of γ_D. These constraints are expressed mathematically as

$$x_1(t_f) = 0; \quad x_3(t_f) = \gamma_D; \quad |x_{(2i+2)}(t_{f_i})| \geq R_i, \quad \forall i = 1, \ldots, N \tag{11}$$

where γ_D is the desired impact angle, and R_i is the desired minimum distance from the ith obstacle.

Remark 1: For derivation of the guidance law, the obstacle–missile distance at the time instant when the missile passes the obstacle is approximated by the distance perpendicular to the LOS. However, there is a small difference between these two distances that can be compensated for during the implementation of the guidance command. This compensation can be done by modifying the desired distances from the obstacles based on the LOS angle of the missile with respect to the obstacles.

III. Guidance Law Derivation

In this section, the problem is first converted to a reduced-order problem using zero-effort transformations [31], and then the guidance designs are performed to satisfy the objectives.

A. Order Reduction

To reduce the system order, the concept of zero-effort transformation is used. The zero-effort transformations of the system states with known target information are given by [3,32]

$$Z_1 = z + (t_f - t)\dot{z} + \frac{1}{2}(t_f - t)^2 a_{TN} \approx t_{\mathrm{go}}^2 V_c \dot{\theta} + \frac{1}{2} t_{\mathrm{go}}^2 a_{TN} \tag{12a}$$

$$Z_2 = \gamma + \frac{a_{TN}(t_f - t)}{V_T'} \approx \gamma_M + \gamma_T + \frac{t_{\mathrm{go}} a_{TN}}{V_T'} = \gamma_M + \gamma_T + \frac{t_{\mathrm{go}} a_T}{V_T} \tag{12b}$$

$$Z_{io} = \begin{cases} z_{io} + (t_{f_i} - t)\dot{z}_{io} \approx t_{\mathrm{go}_i}^2 V_M \dot{\theta}_{o_i} & t \leq t_{f_i} \\ \text{Constant} = Z_{io}(t_{f_i}) & t > t_{f_i} \end{cases}, \quad \forall i = 1, \ldots, N \tag{12c}$$

The dynamics of these zero-effort quantities can be written as

$$\dot{Z}_1 = -(t_f - t)a_{MN} \tag{13a}$$

$$\dot{Z}_2 = \frac{a_{MN}}{V_M'} = \frac{a_M}{V_M} \tag{13b}$$

$$\dot{Z}_{io} = \begin{cases} -(t_{f_i} - t)a_{MN}, & t \leq t_{f_i} \\ 0, & t > t_{f_i} \end{cases}, \quad \forall i = 1, \ldots, N \tag{13c}$$

This transformation reduces the system order from $(2N+3)$ to $(N+2)$.

Regarding the reduced-order problem, the problem of guidance design stated in Sec. II.B now reduces to a problem with the same cost function but reduced-order system dynamics given by Eq. (13). The terminal conditions written in terms of the new states as

$$Z_1(t_f) = 0; \quad Z_2(t_f) = \gamma_D; \quad |Z_{io}(t_f)| \geq R_i \quad \forall i = 1, \ldots, N \tag{14}$$

must be satisfied.

B. Solution of Reduced-Order Problem

To find the solution for the reduced-order problem, an auxiliary problem is presented to determine the missile lateral acceleration, which minimizes the total control effort and satisfies the constraints

$$Z_1(t_f) = 0, \quad Z_2(t_f) = Z_2^d, \quad Z_{io}(t_f) = Z_{io}^d, \quad \forall i = 1, \ldots, N \tag{15}$$

with arbitrary Z_{io}^d considered. By using the system dynamics of Eq. (13), the constraints of Eq. (15) can be rewritten as

$$Z_1(t_0) - \int_0^{t_f} (t_f - \tau) a_{MN}\, \mathrm{d}\tau = 0 \tag{16a}$$

$$Z_2(t_0) + \int_0^{t_f} \frac{a_{MN}}{V'_M}\, \mathrm{d}\tau = Z_2^d \tag{16b}$$

$$Z_{io}(t_0) - \int_0^{t_{f_i}} (t_{f_i} - \tau) a_{MN}\, \mathrm{d}\tau = Z_{io}^d \quad \forall i = 1, \ldots, N \tag{16c}$$

Using Theorem 1, given in Appendix A, if a_{MN} is optimal, then there exist $(N+2)$ constants λ_1, λ_2, and $\lambda_{io}\ \forall i = 1, \ldots, N$ and such that the missile lateral acceleration a_{MN} can be written as

$$a_{MN} = \begin{cases} \lambda_1(t_f - t) + \lambda_2/V'_M + \sum_{i=1}^{i=N} \lambda_{io}(t_{f_i} - t) & t \le t_{f_1} \\ \lambda_1(t_f - t) + \lambda_2/V'_M + \sum_{i=j}^{i=N} \lambda_{io}(t_{f_i} - t) & t_{f_j} \le t \le t_{f_N}\ \forall j = 1 \ldots N \\ \lambda_1(t_f - t) + \lambda_2/V'_M & t \ge t_{f_N} \end{cases} \tag{17}$$

By inserting a_{MN} from Eq. (17) into Eq. (16) and integrating, we obtain

$$\begin{aligned} Z_1(t_0) &= \lambda_1 \int_{t_0}^{t_f} (t_f - \tau)^2\, \mathrm{d}\tau + \frac{\lambda_2}{V'_M} \int_{t_0}^{t_f} (t_f - \tau)\, \mathrm{d}\tau \\ &\quad + \sum_{i=1}^{i=N} \lambda_{io} \int_{t_0}^{t_{f_i}} (t_f - \tau)(t_{f_i} - \tau)\, \mathrm{d}\tau \\ Z_2^d - Z_2(t_0) &= \frac{\lambda_1}{V'_M} \int_{t_0}^{t_f} (t_f - \tau)\, \mathrm{d}\tau + \frac{\lambda_2}{(V'_M)^2} \int_{t_0}^{t_f} \mathrm{d}\tau \\ &\quad + \sum_{i=1}^{i=N} \frac{\lambda_{io}}{V'_M} \int_{t_0}^{t_{f_i}} (t_{f_i} - \tau)\, \mathrm{d}\tau \\ Z_{jo}(t_0) - Z_{jo}^d &= \lambda_1 \int_{t_0}^{t_{f_j}} (t_f - \tau)(t_{f_j} - \tau)\, \mathrm{d}\tau + \frac{\lambda_2}{V'_M} \int_{t_0}^{t_{f_j}} (t_{f_j} - \tau)\, \mathrm{d}\tau \\ &\quad + \sum_{i=1}^{i=N} \lambda_{io} \int_{t_0}^{t_{f_{ij}}} (t_{f_i} - \tau)(t_{f_j} - \tau)\, \mathrm{d}\tau \end{aligned} \tag{18}$$

where

$$t_{f_{ij}} = \min(t_{f_i}, t_{f_j})$$

and both $i, j = 1, \ldots, N$. On evaluating the integrals in Eq. (18), it reduces to

$$G \begin{bmatrix} \boldsymbol{\lambda}_I \\ \boldsymbol{\lambda}_o \end{bmatrix} = \begin{bmatrix} \boldsymbol{Z}_I \\ \boldsymbol{Z}_o - \boldsymbol{Z}_o^d \end{bmatrix}, \qquad G = \begin{bmatrix} G_1 & G_{12} \\ G_{12}^T & G_2 \end{bmatrix} \tag{19}$$

where

$$\boldsymbol{Z}_I = \begin{bmatrix} Z_1(t_0) \\ Z_2^d - Z_2(t_0) \end{bmatrix}, \quad \boldsymbol{\lambda}_I = \begin{bmatrix} \lambda_1 \\ \lambda_2 \end{bmatrix}, \quad G_1 = \begin{bmatrix} \frac{t_{\mathrm{go}}^3}{3} & \frac{t_{\mathrm{go}}^2}{2V'_M} \\ \frac{t_{\mathrm{go}}^2}{2V'_M} & \frac{t_{\mathrm{go}}}{(V'_M)^2} \end{bmatrix} \tag{20a}$$

$$G_{12} = \begin{bmatrix} \frac{t_{\mathrm{go}} t_{\mathrm{go}_1}^2}{2} - \frac{t_{\mathrm{go}_1}^3}{6} & \cdots & \frac{t_{\mathrm{go}} t_{\mathrm{go}_i}^2}{2} - \frac{t_{\mathrm{go}_i}^3}{6} & \cdots & \frac{t_{\mathrm{go}} t_{\mathrm{go}_N}^2}{2} - \frac{t_{\mathrm{go}_N}^3}{6} \\ \frac{t_{\mathrm{go}_1}^2}{2V'_M} & \cdots & \frac{t_{\mathrm{go}_i}^2}{2V'_M} & \cdots & \frac{t_{\mathrm{go}_N}^2}{2V'_M} \end{bmatrix} \tag{20b}$$

$$\boldsymbol{\lambda}_o = [\lambda_{1o} \quad \cdots \quad \lambda_{io} \quad \cdots \quad \lambda_{No}]^T \tag{20c}$$

$$\boldsymbol{Z}_o = [Z_{1o}(t_0) \quad \cdots \quad Z_{io}(t_0) \quad \cdots \quad Z_{No}(t_0)]^T \tag{20d}$$

$$\boldsymbol{Z}_o^d = [Z_{1o}^d \quad \cdots \quad Z_{io}^d \quad \cdots \quad Z_{No}^d]^T \tag{20e}$$

$$[G_2]_{ij} = [G_2]_{ji} = \frac{t_{\mathrm{go}_j} t_{\mathrm{go}_i}^2}{2} - \frac{t_{\mathrm{go}_i}^3}{6} \quad \forall i \le j;\ i = 1, \ldots, N,\ j = 1, \ldots, N \tag{20f}$$

From Eq. (19), the coefficients $\boldsymbol{\lambda}_I$ and $\boldsymbol{\lambda}_o$ (also called Lagrange multipliers) can be obtained as

$$\begin{bmatrix} \boldsymbol{\lambda}_I \\ \boldsymbol{\lambda}_o \end{bmatrix} = G^{-1} \begin{bmatrix} \boldsymbol{Z}_I \\ \boldsymbol{Z}_o - \boldsymbol{Z}_o^d \end{bmatrix}; \quad G^{-1} \triangleq \begin{bmatrix} G_{1_I} & G_{12_I} \\ G_{12_I}^T & G_{2_I} \end{bmatrix} \tag{21}$$

On computing the total control effort, using Eqs. (10) and (17), and performing some simplifications, we get

$$\begin{aligned} \int_0^{t_f} a_{MN}^2\, \mathrm{d}t &= \begin{bmatrix} \boldsymbol{\lambda}_I \\ \boldsymbol{\lambda}_o \end{bmatrix}^T G \begin{bmatrix} \boldsymbol{\lambda}_I \\ \boldsymbol{\lambda}_o \end{bmatrix} \\ &= \begin{bmatrix} \boldsymbol{Z}_I \\ \boldsymbol{Z}_o - \boldsymbol{Z}_o^d \end{bmatrix}^T \begin{bmatrix} G_{1_I} & G_{12_I} \\ G_{12_I}^T & G_{2_I} \end{bmatrix} \begin{bmatrix} \boldsymbol{Z}_I \\ \boldsymbol{Z}_o - \boldsymbol{Z}_o^d \end{bmatrix} \end{aligned} \tag{22}$$

Now, the desired zero-effort miss (ZEM) distances corresponding to all obstacles $\boldsymbol{Z}_o^d \in \mathbb{R}^N$ need to be determined such that they minimize the total control effort under the constraints of collision avoidance with all the obstacles; that is, $|\boldsymbol{Z}_{io}^d| \ge R_i\ \forall i = 1, \ldots, N$. This problem can be written mathematically as

$$\boldsymbol{Z}_o^{d\star} = \arg\min_{Z_o^d \in S} \begin{bmatrix} \boldsymbol{Z}_I \\ \boldsymbol{Z}_o - \boldsymbol{Z}_o^d \end{bmatrix}^T \begin{bmatrix} G_{1_I} & G_{12_I} \\ G_{12_I}^T & G_{2_I} \end{bmatrix} \begin{bmatrix} \boldsymbol{Z}_I \\ \boldsymbol{Z}_o - \boldsymbol{Z}_o^d \end{bmatrix} \tag{23}$$

where

$$\boldsymbol{S} = \{\boldsymbol{Z}_o^d \in \mathbb{R}^N | \boldsymbol{Z}_o^d(i) \ge R_i,\ \forall\ 1, \ldots, N\} \tag{24}$$

This optimization problem reduces to the problem of optimizing a convex function over the union of several convex domains. By computing the optimal values $\boldsymbol{Z}_o^{d\star}$, the values of Lagrange multipliers can be obtained using Eq. (21).

Proposition 1: The optimization problem, given by Eq. (23), is equivalent to the reduced form given by

$$\boldsymbol{Z}_o^{d\star} = \arg\min_{Z_o^d \in S} (\boldsymbol{Z}_o^d - \boldsymbol{Z}_c)^T G_{2_I} (\boldsymbol{Z}_o^d - \boldsymbol{Z}_c) \tag{25}$$

where the vector $\boldsymbol{Z}_c$ is defined as

$$\boldsymbol{Z}_c = \boldsymbol{Z}_o + G_{2_I}^{-1} G_{12_I}^T \boldsymbol{Z}_I \tag{26}$$

Proof: The proof of this proposition can be found in Appendix B. □

Now, the optimal solution $\boldsymbol{Z}_o^{d\star}$ of the optimization problem, given by Eq. (25), can be expressed in terms of the generalized dead-zone function, which is defined in Appendix D as

$$G_{2_I}(\boldsymbol{Z}_o^{d\star} - \boldsymbol{Z}_c) = \Psi_{S, G_{2_I}}(\boldsymbol{Z}_c) \tag{27}$$

On some algebraic manipulations of Eq. (27), we obtain

$$\begin{aligned}\boldsymbol{Z}_o - \boldsymbol{Z}_o^{d\star} &= -G_{2_I}^{-1}\Psi_{S,G_{2_I}}(\boldsymbol{Z}_c) - (\boldsymbol{Z}_c - \boldsymbol{Z}_o)\\ &= -G_{2_I}^{-1}\Big[\Psi_{S,G_{2_I}}(\boldsymbol{Z}_c) + G_{12_I}^T\boldsymbol{Z}_I\Big] \end{aligned}\tag{28}$$

Proposition 2: By using the optimal values for the desired zero-effort miss distances with respect to the obstacles $\boldsymbol{Z}_o^{d\star}$ in Eq. (21), the coefficients $\boldsymbol{\lambda}_I$ and $\boldsymbol{\lambda}_o$ can be obtained, and those are given by

$$\begin{bmatrix}\boldsymbol{\lambda}_I\\ \boldsymbol{\lambda}_o\end{bmatrix} = \begin{bmatrix} G_1^{-1}\boldsymbol{Z}_I + G_1^{-1}G_{12}\Psi_{S,G_{2_I}}(\boldsymbol{Z}_c)\\ -\Psi_{S,G_{2_I}}(\boldsymbol{Z}_c)\end{bmatrix}\tag{29}$$

Proof: The proof of this proposition can be found in Appendix C. □

To derive the expression for the guidance command, these values of λ can be substituted in Eq. (17). By defining $\boldsymbol{C}_1 = [t_{go} 1/V_M']$ and $\boldsymbol{C}_2 = [t_{go_1} \dots t_{go_i} \dots t_{go_N}]$, the guidance command can be expressed as

$$\begin{aligned} a_{MN} &= \boldsymbol{C}_1\boldsymbol{\lambda}_I + \boldsymbol{C}_2\boldsymbol{\lambda}_o\\ &= \boldsymbol{C}_1\Big[G_1^{-1}\boldsymbol{Z}_I + G_1^{-1}G_{12}\Psi_{S,G_{2_I}}(\boldsymbol{Z}_c)\Big] - \boldsymbol{C}_2\Psi_{S,G_{2_I}}(\boldsymbol{Z}_c)\\ &= \begin{bmatrix} t_{go}\\ 1/V_M'\end{bmatrix}^T \begin{bmatrix} \frac{12}{t_{go}^3} & -\frac{6V_M'}{t_{go}^2}\\ -\frac{6V_M'}{t_{go}^2} & \frac{4(V_M')^2}{t_{go}}\end{bmatrix}\begin{bmatrix} Z_1(t_0)\\ Z_2^d - Z_2(t_0)\end{bmatrix}\\ &\quad + \Big[\boldsymbol{C}_1 G_1^{-1}G_{12} - \boldsymbol{C}_2\Big]\Psi_{S,G_{2_I}}(\boldsymbol{Z}_c)\\ &= \frac{6Z_1(t_0)}{t_{go}^2} + \frac{2V_M'(Z_2(t_0) - Z_2^d)}{t_{go}} + \Big[\boldsymbol{C}_1 G_1^{-1}G_{12} - \boldsymbol{C}_2\Big]\Psi_{S,G_{2_I}}(\boldsymbol{Z}_c)\end{aligned}\tag{30}$$

On evaluating $\boldsymbol{C}_1 G_1^{-1}G_{12}$, we get

$$\begin{aligned}\boldsymbol{C}_1 G_1^{-1}G_{12} &= \begin{bmatrix}\frac{6}{t_{go}^2}\\ -\frac{2V_M'}{t_{go}}\end{bmatrix}^T\begin{bmatrix} \frac{t_{go}t_{go_1}^2}{2} - \frac{t_{go_1}^3}{6} & \dots & \frac{t_{go}t_{go_i}^2}{2} - \frac{t_{go_i}^3}{6} & \dots & \frac{t_{go}t_{go_N}^2}{2} - \frac{t_{go_N}^3}{6}\\ \frac{t_{go_1}^2}{2V_M'} & \dots & \frac{t_{go_i}^2}{2V_M'} & \dots & \frac{t_{go_N}^2}{2V_M'}\end{bmatrix}\\ &= \begin{bmatrix}\frac{t_{go_1}^2(2t_{go} - t_{go_1})}{t_{go}^2} & \dots & \frac{t_{go_i}^2(2t_{go} - t_{go_i})}{t_{go}^2} & \dots & \frac{t_{go_N}^2(2t_{go} - t_{go_N})}{t_{go}^2}\end{bmatrix}\end{aligned}\tag{31}$$

from which we can further simplify $\boldsymbol{C}_1 G_1^{-1}G_{12} - \boldsymbol{C}_2$ as

$$\boldsymbol{C}_1 G_1^{-1}G_{12} - \boldsymbol{C}_2 = -\begin{bmatrix}\frac{t_{go_1}\Delta_1^2}{t_{go}^2} & \dots & \frac{t_{go_i}\Delta_i^2}{t_{go}^2} & \dots & \frac{t_{go_N}\Delta_N^2}{t_{go}^2}\end{bmatrix}\tag{32}$$

where $\Delta_i = t_{go} - t_{go_i}, \forall i = 1, \dots, N$ are the same as those defined in Eq. (9). On using Eq. (32), the guidance command in Eq. (30) can be written as

$$a_{MN} = \frac{6Z_1(t_0)}{t_{go}^2} + \frac{2V_M'(Z_2(t_0) - Z_2^d)}{t_{go}} - a_{MNo}\tag{33}$$

where

$$a_{MNo} = \frac{1}{t_{go}^2}\Big[t_{go_1}\Delta_1^2 \quad \dots \quad t_{go_i}\Delta_i^2 \quad \dots \quad t_{go_N}\Delta_N^2\Big]\Psi_{S,G_{2_I}}(\boldsymbol{Z}_c)\tag{34}$$

The first and second components of the guidance command, given by Eq. (33), correspond to interception of the target and the achievement of the desired impact angle, respectively. The term a_{MNo} in Eqs. (33) and (34) is the component of the guidance command responsible for detecting obstacles and generating corrective maneuvers for the avoidance of obstacles. It is important to note that the term a_{MNo} contains a term corresponding to each obstacle. Furthermore, each obstacle's contributing terms have a similar structure with respect to their corresponding time to go.

The guidance command in Eq. (33) can be approximated in terms of guidance variables as

$$a_{MN} = -6V_r\dot{\theta} + \left(3 + \frac{2V_M'}{V_T'}\right)a_{TN} + \left(\frac{2V_M'}{t_{go}}\right)(\gamma_M + \gamma_T - \gamma_D) - a_{MNo}\tag{35}$$

It can also be noted from Eq. (35) that the guidance command has a form similar to that of the augmented PN guidance law with a navigation constant equal to six.

Remark 2: For the case where no obstacles are present in the engagement environment, the term a_{MNo} disappears from Eq. (35); consequently, the guidance command is the same as that obtained in [3].

Remark 3: The proposed guidance law given by Eq. (35) is derived for a general case of multiple obstacles. Its implementation depends on the computation of the dead-zone function, which in turn relies on obtaining the optimal solution of the multivariable quadratic optimization problem. The main computational burden of the proposed guidance scheme comes from the optimal solution required to define the dead-zone function in Eq. (34).

Remark 4: It is worthy to note here that, by deriving the guidance law, there is no restriction imposed on the value of the desired impact angle. This allows the proposed guidance scheme to remain applicable for the arbitrary impact angle as long as other assumptions remain valid.

It is important to note from Eq. (34) that the maneuvers required for obstacle avoidance depend on the term $\Psi_{S,G_{2_I}}(\boldsymbol{Z}_c)$. If the obstacles are far away from the missile satisfying $\boldsymbol{Z}_c \in \boldsymbol{S}$, then $\Psi_{S,G_{2_I}}(\boldsymbol{Z}_c) = 0$. As a result, the missile does not require any maneuver for obstacle avoidance. On the other hand, if the missile is close enough to the obstacle (that is, $\boldsymbol{Z}_c \notin \boldsymbol{S}$), then $\Psi_{S,G_{2_I}}(\boldsymbol{Z}_c)$ has a nonzero value; and the required maneuvers for obstacle avoidance can be obtained from Eq. (34). Therefore, obstacle collision detection depends on the value of Z_c. This analysis clearly shows that both obstacle detection and the generation of obstacle-avoidance maneuvers are performed by the dead-zone function $\Psi_{S,G_{2_I}}(\boldsymbol{Z}_c)$. This is different from the algorithms in [22–26], which performed these two actions independently. Due to the inherent integration of these two steps, the proposed guidance law avoids a possible performance degradation, which may result from the decoupled actions of obstacle detection and obstacle avoidance.

Remark 5: The chances of collision with obstacles never arise if the obstacle are sufficiently far from the missile–target collision course. In such a case, the guidance strategy for the missile needs to focus only on interception of the target with a desired intercept angle. The proposed guidance strategy in Eq. (35) has this feature due to the presence of a_{MNo}. The dead-zone function nullifies the effect of distant obstacles. The situation becomes critical only when the obstacle is near and around the collision course of the missile. This justifies our assumption that the obstacles are close to the collision course for guidance derivation.

IV. Particular Cases

In this section, the guidance law for the special cases of engagement scenarios with one and two obstacles is presented.

A. Case of Single Obstacle

In this case, it is assumed that there is only one obstacle present in the environment, with the minimum distance required to avoid the obstacle being R_1. For this case, the matrices G_{12} and G_2, as well as the vector $\boldsymbol{C}_2$, reduce to

$$G_{12}^T = \begin{bmatrix}\frac{t_{go}t_{go_1}^2}{2} - \frac{t_{go_1}^3}{6} & \frac{t_{go_1}^2}{2V_M'}\end{bmatrix}, \qquad G_2 = \frac{t_{go_1}^3}{3}, \qquad \boldsymbol{C}_2 = t_{go_1}\tag{36}$$

On substituting the matrices and vector given in Eq. (36) in the matrix G, we obtain

$$G=\begin{bmatrix}\frac{t_{\text{go}}^3}{3} & \frac{t_{\text{go}}^2}{2V_M'} & \frac{t_{\text{go}}t_{\text{go}_1}^2}{2}-\frac{t_{\text{go}_1}^3}{6}\\ \frac{t_{\text{go}}^2}{2V_M'} & \frac{t_{\text{go}}}{(V_M')^2} & \frac{t_{\text{go}_1}^2}{2V_M'}\\ \frac{t_{\text{go}}t_{\text{go}_1}^2}{2}-\frac{t_{\text{go}_1}^3}{6} & \frac{t_{\text{go}_1}^2}{2V_M'} & \frac{t_{\text{go}_1}^3}{3}\end{bmatrix} \tag{37}$$

Note that the matrix G_{2_I} and the set $\boldsymbol{S}_{R_1}$ in this case are given by

$$G_{2_I}=\frac{3t_{\text{go}}^3}{t_{\text{go}_1}^3\Delta_1^3}, \qquad \boldsymbol{S}_{R_1}=\left\{Z_{1o}^d\in\mathbb{R}\,|\,|Z_{1o}^d|>R_1\right\} \tag{38}$$

The guidance command, for time $t\le t_{f_1}$, with a single obstacle, is given by

$$a_{MN}=-6V_r\dot{\theta}+\left(3+\frac{2V_M'}{V_T'}\right)a_{TN}+\left(\frac{2V_M'}{t_{\text{go}}}\right)(\gamma_M+\gamma_T-\gamma_D) - \underbrace{(t_{\text{go}_1}\Delta_1^2/t_{\text{go}}^2)\Psi_{S,G_{2_I}}(Z_{1c})}_{a_{MNo}} \tag{39}$$

where $\Delta_1=t_{\text{go}}-t_{\text{go}_1}$, and the function $\Psi_{S,G_{2_I}}(Z_{1c})$ is defined in Appendix E. It is important to note that a_{MNo} in Eq. (39) reduces, using the definition of $\Psi_{R_1}(Z_{1c})$ in Appendix E as

$$a_{MNo}=-\frac{3t_{\text{go}}}{t_{\text{go}_1}^2\Delta_1}\psi_{R_1}(Z_{1c}) \tag{40}$$

The term Z_{1c} comes from Eq. (26) and, after some algebraic manipulations, is given by

$$Z_{1c}=Z_{1o}(t_0)-\frac{t_{\text{go}_1}^2(t_{\text{go}_1}+3\Delta_1)}{t_{\text{go}}^3}Z_1(t_0)-\frac{t_{\text{go}_1}^2V_M'\Delta_1}{t_{\text{go}}^2}(Z_2(t_0)-Z_2^d)$$

which can be further expressed in terms of guidance variables as

$$Z_{1c}=t_{\text{go}_1}^2\left[V_M\dot{\theta}_o+\left(1+\frac{2\Delta_1}{t_{\text{go}}}\right)V_r\dot{\theta}-a_{TN}\left\{\frac{1}{2}+\frac{\Delta_1}{t_{\text{go}}}\left(1+\frac{V_M'}{V_T'}\right)\right\} -\frac{V_M'\Delta_1}{t_{\text{go}}^2}(\gamma_M+\gamma_T-\gamma_D)\right] \tag{41}$$

For all time instants $t\ge t_{f_1}$, the guidance command reduces to

$$a_{MN}=6V_c\dot{\theta}+\left(3+\frac{2V_M'}{V_T'}\right)a_{TN}+\left(\frac{2V_M'}{t_{\text{go}}}\right)(\gamma_M+\gamma_T-\gamma_D) \tag{42}$$

Remark 6: The guidance command, given by Eq. (39), has a structure similar to that obtained in [33], with an additional term for the impact angle error correction. Note that the guidance laws proposed in [33] address the problems of only target interception and, with additional constraint on the rendezvous, for an engagement with a single obstacle. However, in this paper, in addition to target interception, an intercept angle constraint is imposed. Moreover, this paper provides a generic derivation of guidance laws in the presence of multiple obstacles.

B. Case of Two Obstacles

The minimum distances required to avoid obstacles 1 and 2 are denoted by R_1 and R_2, respectively. For this case, the matrix G_1 remains the same, whereas the other matrices in Eq. (19) are given by

$$G_{12}=\begin{bmatrix}\frac{t_{\text{go}}t_{\text{go}_1}^2}{2}-\frac{t_{\text{go}_1}^3}{6} & \frac{t_{\text{go}}t_{\text{go}_2}^2}{2}-\frac{t_{\text{go}_2}^3}{6}\\ \frac{t_{\text{go}_1}^2}{2V_M'} & \frac{t_{\text{go}_2}^2}{2V_M'}\end{bmatrix},$$

$$G_2=\begin{bmatrix}\frac{t_{\text{go}_1}^3}{3} & \frac{t_{\text{go}_2}t_{\text{go}_1}^2}{2}-\frac{t_{\text{go}_1}^3}{6}\\ \frac{t_{\text{go}_2}t_{\text{go}_1}^2}{2}-\frac{t_{\text{go}_1}^3}{6} & \frac{t_{\text{go}_2}^3}{3}\end{bmatrix} \tag{43}$$

The matrix G then becomes

$$G=\begin{bmatrix}\frac{t_{\text{go}}^3}{3} & \frac{t_{\text{go}}^2}{2V_M'} & \frac{t_{\text{go}}t_{\text{go}_1}^2}{2}-\frac{t_{\text{go}_1}^3}{6} & \frac{t_{\text{go}}t_{\text{go}_2}^2}{2}-\frac{t_{\text{go}_2}^3}{6}\\ \frac{t_{\text{go}}^2}{2V_M'} & \frac{t_{\text{go}}}{(V_M')^2} & \frac{t_{\text{go}_1}^2}{2V_M'} & \frac{t_{\text{go}_2}^2}{2V_M'}\\ \frac{t_{\text{go}}t_{\text{go}_1}^2}{2}-\frac{t_{\text{go}_1}^3}{6} & \frac{t_{\text{go}_1}^2}{2V_M'} & \frac{t_{\text{go}_1}^3}{3} & \frac{t_{\text{go}_2}t_{\text{go}_1}^2}{2}-\frac{t_{\text{go}_1}^3}{6}\\ \frac{t_{\text{go}}t_{\text{go}_2}^2}{2}-\frac{t_{\text{go}_2}^3}{6} & \frac{t_{\text{go}_2}^2}{2V_M'} & \frac{t_{\text{go}_2}t_{\text{go}_1}^2}{2}-\frac{t_{\text{go}_1}^3}{6} & \frac{t_{\text{go}_2}^3}{3}\end{bmatrix} \tag{44}$$

and the components of matrix G^{-1} are given by

$$G_{1_I}=\begin{bmatrix}\frac{12(3t_{\text{go}2}\Delta_2+t_{\text{go}}\Delta)}{\Delta_2^3(3t_{\text{go}2}\Delta_1+t_{\text{go}}\Delta)} & -\frac{6V_M'(t_{\text{go}}\Delta+t_{\text{go}2}(\Delta_1+2\Delta_2)}{\Delta_2^2(3t_{\text{go}2}\Delta_1+t_{\text{go}}\Delta)}\\ -\frac{6V_M'(t_{\text{go}}\Delta+t_{\text{go}2}(\Delta_1+2\Delta_2)}{\Delta_2^2(3t_{\text{go}2}\Delta_1+t_{\text{go}}\Delta)} & \frac{4(V_M')^2(t_{\text{go}}\Delta+t_{\text{go}2}(2\Delta_1+\Delta_2))}{\Delta_2^2(3t_{\text{go}2}\Delta_1+t_{\text{go}}\Delta)}\end{bmatrix}$$

$$G_{12_I}=\begin{bmatrix}\frac{18t_{\text{go}2}^2}{t_{\text{go}1}\Delta_2\Delta(3t_{\text{go}2}\Delta_1+t_{\text{go}}\Delta)} & -\frac{6[(t_{\text{go}}+2\Delta_1)(t_{\text{go}}\Delta+t_{\text{go}_2}\Delta_2)-t_{\text{go}_2}^2\Delta_1]}{\Delta_2^3\Delta(3t_{\text{go}2}\Delta_1+t_{\text{go}}\Delta)}\\ -\frac{6V_M't_{\text{go}2}^2}{t_{\text{go}1}\Delta(3t_{\text{go}2}\Delta_1+t_{\text{go}}\Delta)} & \frac{6V_M'\Delta_1(t_{\text{go}}\Delta+t_{\text{go}2}\Delta_1)}{\Delta_2^2\Delta(3t_{\text{go}2}\Delta_1+t_{\text{go}}\Delta)}\end{bmatrix}$$

$$G_{2_I}=\begin{bmatrix}\frac{12t_{\text{go}}t_{\text{go}2}^3}{t_{\text{go}1}^3\Delta^2(3t_{\text{go}2}\Delta_1+t_{\text{go}}\Delta)} & -\frac{6t_{\text{go}}(t_{\text{go}}\Delta+2t_{\text{go}2}\Delta_1)}{t_{\text{go}1}\Delta_2\Delta^2(3t_{\text{go}2}\Delta_1+t_{\text{go}}\Delta)}\\ -\frac{6t_{\text{go}}(t_{\text{go}}\Delta+2t_{\text{go}2}\Delta_1)}{t_{\text{go}1}\Delta_2\Delta^2(3t_{\text{go}2}\Delta_1+t_{\text{go}}\Delta)} & \frac{12t_{\text{go}}\Delta_1^3}{\Delta_2^3\Delta^2(3t_{\text{go}2}\Delta_1+t_{\text{go}}\Delta)}\end{bmatrix} \tag{45}$$

where $\Delta_1=t_{\text{go}}-t_{\text{go}_1}$, $\Delta_2=t_{\text{go}}-t_{\text{go}_2}$, and $\Delta=t_{\text{go}_2}-t_{\text{go}_1}$.

For this case, the guidance command for time $t\le t_{f_1}$ can be written using Eqs. (33) and (35) in terms of the guidance variables as

$$a_{MN}^{\star}=-6V_r\dot{\theta}+\left[3+\frac{2V_M'}{V_T'}\right]a_{TN}+\left[\frac{2V_M'}{t_{\text{go}}}\right](\gamma_M+\gamma_T-\gamma_D) - \underbrace{(1/t_{\text{go}}^2)\begin{bmatrix}t_{\text{go}_1}\Delta_1^2\\ t_{\text{go}_2}\Delta_2^2\end{bmatrix}^T\Psi_{S,G_{2_I}}(\boldsymbol{Z}_c)}_{a_{MNo}} \tag{46}$$

where the set $\boldsymbol{S}_{R_1,R_2}$ for this case is defined as

$$\boldsymbol{S}_{R_1,R_2}=\left\{[Z_{1o}^d\quad Z_{2o}^d]^T\in\mathbb{R}^2\,|\,|Z_{1o}^d|>R_1,|Z_{2o}^d|>R_2\right\} \tag{47}$$

The function $\Psi_{S,G_{2_I}}(\boldsymbol{Z}_c)$ is a two-dimensional dead-zone function. Although an explicit formula for the computation of this function would be extremely complex, in Appendix F, we present an algorithm for computing this function that requires modest computational resources. The term $\boldsymbol{Z}_c\in\mathbb{R}^2$, obtained by substituting Eq. (45) in Eq. (26), is given by

$$\boldsymbol{Z}_c=\begin{bmatrix}Z_{1c}\\ Z_{2c}\end{bmatrix} =\begin{bmatrix}Z_{1o}(t_0)-\frac{t_{\text{go}_1}^2(3\Delta_1+t_{\text{go}_1})}{t_{\text{go}}^3}Z_1(t_0)-\frac{\Delta_1V_M't_{\text{go}_1}^2}{t_{\text{go}}^2}(Z_2(t_0)-Z_2^d)\\ Z_{2o}(t_0)-\frac{t_{\text{go}_2}^2(3\Delta_2+t_{\text{go}_2})}{t_{\text{go}}^3}Z_1(t_0)-\frac{\Delta_2V_M't_{\text{go}_2}^2}{t_{\text{go}}^2}(Z_2(t_0)-Z_2^d)\end{bmatrix} \tag{48}$$

Similar to Eq. (41), $\boldsymbol{Z}_c$ can be further expressed in terms of the guidance variables.

Table 1 Simulation parameters

Parameters	Symbols	Values
Missile speed	V_M	400 m/s
Target speed	V_T	400 m/s
Target acceleration	a_T	$2g$
Initial missile–target distance	r	10 km
Initial line-of-sight angle	θ	0 deg
Missile flight-path angle	γ_M	0 deg
Target flight-path angle	γ_T	0 deg

Note that the a_{MNo} term in the guidance command, given by Eq. (46), is not the same as that of the single-obstacle case. However, other components of the guidance command are similar to those of the single-obstacle case. It is also important to note that the guidance commands for the time intervals $t_{f_1} \le t \le t_{f_2}$ and $t \ge t_{f_2}$ remain the same as those for the cases of the single obstacle and no obstacle, respectively.

V. Simulation Study

In this section, the performance of the proposed guidance law is evaluated through numerical simulations using linear as well as nonlinear engagement kinematics. Two types of simulations are performed: the first one considers only a single obstacle, and the second one features two obstacles. In the simulations, both the missile and target are considered to be of ideal dynamics. In the subsequent figures, the circle and star markers denote the start positions of the missiles and the targets, respectively; whereas the diamond markers represent the positions of the obstacles.

A. Single Obstacle

The effect of four different variations in engagement parameters on the performance of the proposed guidance law is investigated in this subsection. These include variations in the desired obstacle-avoidance distance, the desired impact angle, the target maneuvers, and the engagement duration.

The single-obstacle engagement scenario has an obstacle located at the position given by $(X_o, Y_o) = (1500, 200)$ m and a desired impact angle of 60 deg. Simulation parameters and initial conditions are listed in Table 1. Three simulations are performed with linear kinematics for different desired distances from the obstacle: that is, $R_1 = (0, 200, 400\ \mathrm{m})$. The results are shown in Fig. 2, which depicts the trajectories of both the missile and target, the lateral acceleration of the missile, the variation of the relative course of the missile and target, and the zero-effort miss with respect to the obstacle.

Figure 2 shows that the missile is able to intercept the target at the desired impact angle. The missile lateral acceleration profile presented in Fig. 2b shows a piecewise linear profile with respect to time. This is mainly due to the initial focus of the guidance law on obstacle avoidance, and then later toward target interception at the desired impact angle. This change occurs at the time instant when the missile passes the obstacle. It can also be observed that the acceleration demand increases as the required minimum distance from obstacle becomes larger. Consequently, the relative course of the missile and the target, as shown in Fig. 2c, changes fast for a large obstacle-avoidance distance. Also, the constraints on the intercept angle and the desired distance from the obstacle are satisfied as shown in Figs. 2c and 2d, respectively.

To evaluate the performance for different impact angles, simulations were performed with the desired impact angles of 0, 30, 60, and 90 deg. The results for these cases are shown in Fig. 3, depicting the trajectories of the missiles and their lateral accelerations. The obstacle is located in the same position as in Fig. 2, with a desired minimum distance of 400 m. The impact angle criterion is satisfied for all cases. An interesting phenomenon occurs when $\gamma = 90$ deg. Due to the requirement of maintaining a minimum missile–obstacle distance, the missile passes the obstacle on a different side as compared to the trajectories corresponding to the other impact angles.

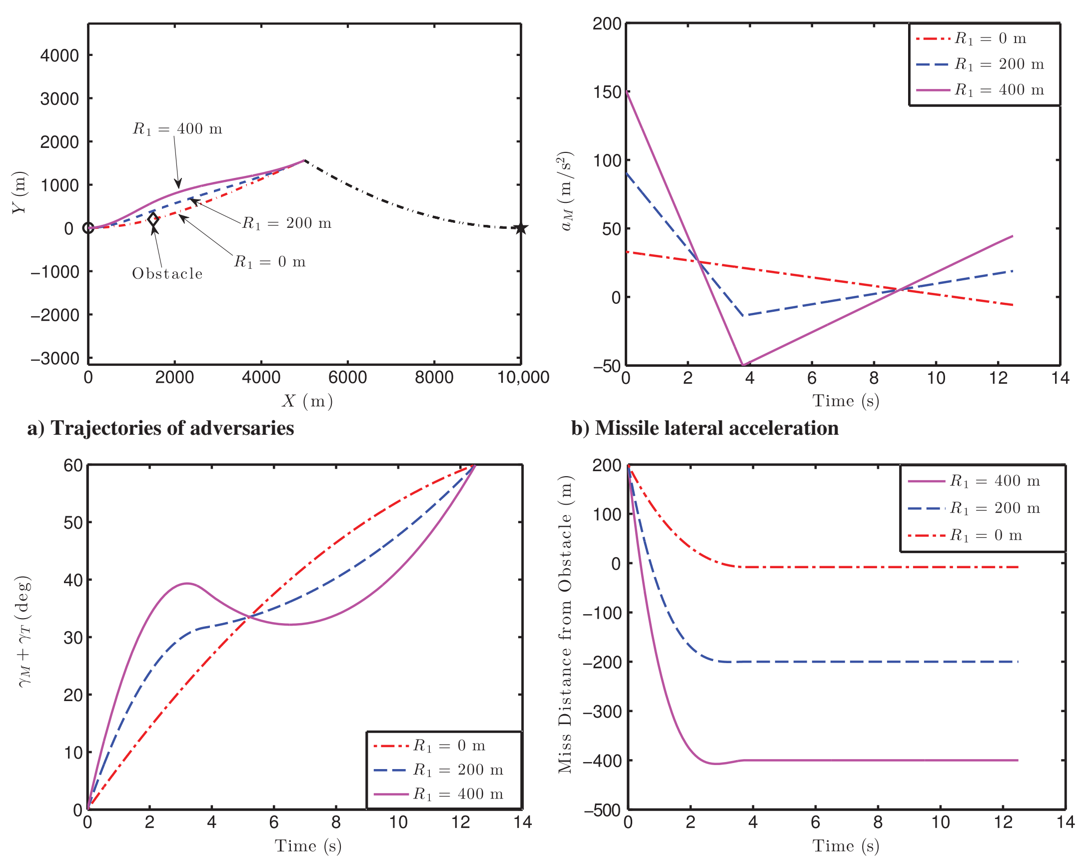

a) Trajectories of adversaries

b) Missile lateral acceleration

c) Variation of relative course of missile and target

d) Zero-effort miss with regard to obstacle

Fig. 2 Interception at an impact angle of 60 deg with a target maneuver of 20 m/s^2 using linear dynamics in the presence of a single obstacle.

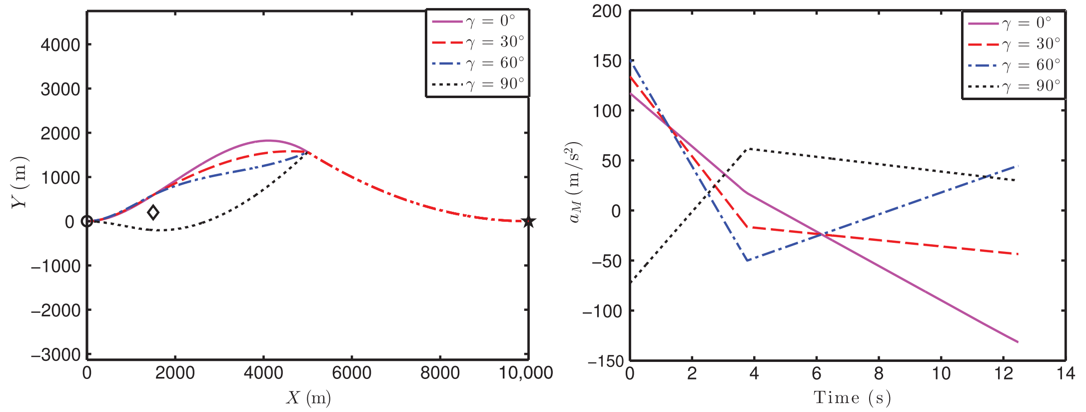

a) Trajectories of adversaries b) Missile lateral accelerations

Fig. 3 Performance of proposed guidance for different desired impact angles.

Simulations have also been carried out for different levels of target maneuvers with a desired impact angle of 45 deg, and the results are shown in Fig. 4. In this case, the target performs maneuvers of $a_T = 1g, 2g, 3g$, and $4g$. The obstacle position and desired minimum distance are identical to the values used in Figs. 2 and 3. The missile is able to achieve the objective in all cases, as shown in Fig. 4a. Note that, for the cases of target maneuvers of $1g$, $2g$, and $3g$, the missile first focuses on obstacle avoidance before aiming for target interception at the desired impact angle. In the case of $4g$, the missile satisfies the constraints of the specified distance from the obstacle; thus, it only maneuvers for interception at the desired impact angle. This can be seen in Fig. 4b because the missile lateral acceleration for $a_T = 4g$ is linear in time, unlike the other three cases where the slope of the lateral acceleration profile changes.

To obtain the performance of the proposed guidance law for various times of flight, simulations were performed for different initial missile–target distances. The results are plotted in Fig. 5, showing the miss distance from the obstacle and the required total control effort. Five different obstacle-avoidance distances of 200, 300, 400, 500, and 600 m are considered. It can be seen that the desired distance is achieved for all the cases and the required control effort increases as the flight time decreases. This is because the missile has to change its course within a small time, and thus needs to perform large maneuvers.

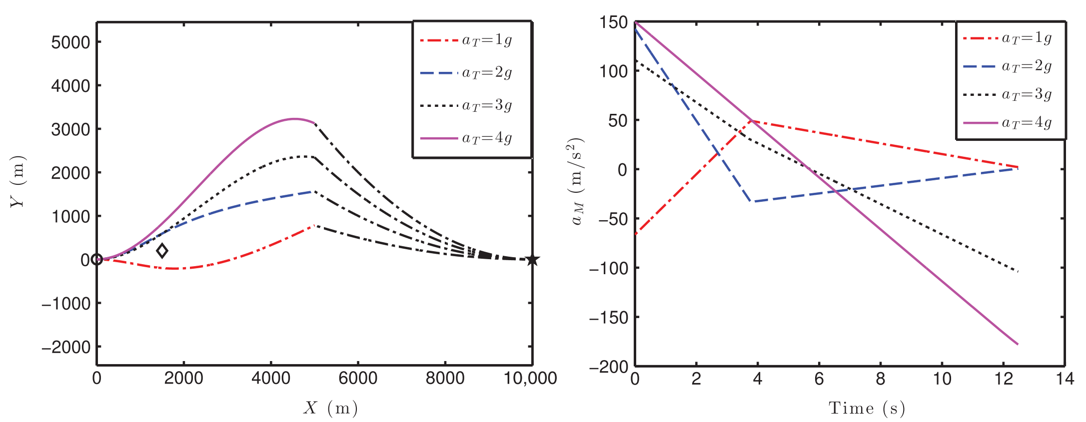

a) Trajectories of adversaries b) Missile lateral accelerations

Fig. 4 Performance of proposed guidance for different levels of target maneuvers with a desired impact angle of 45 deg.

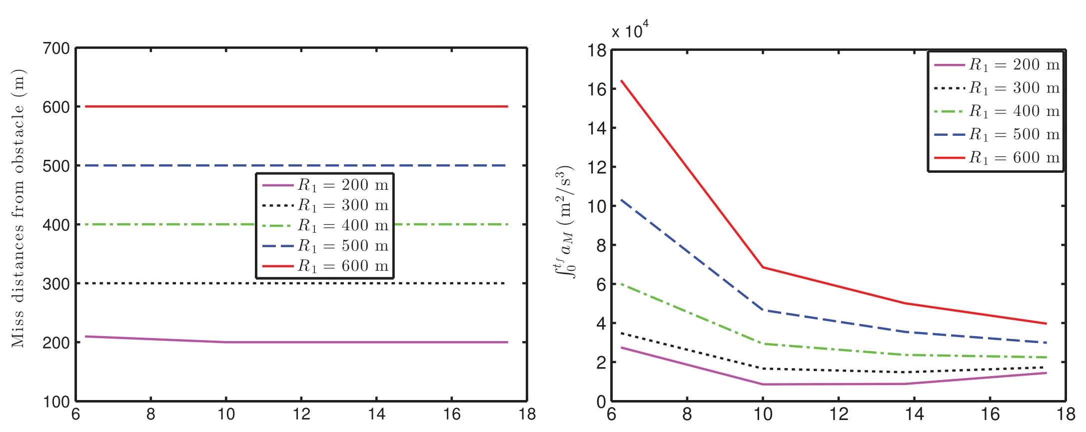

a) Miss distances with respect to obstacle b) Total control efforts of missile

Fig. 5 Performance of proposed guidance with respect to time of flight in the presence of one obstacle.

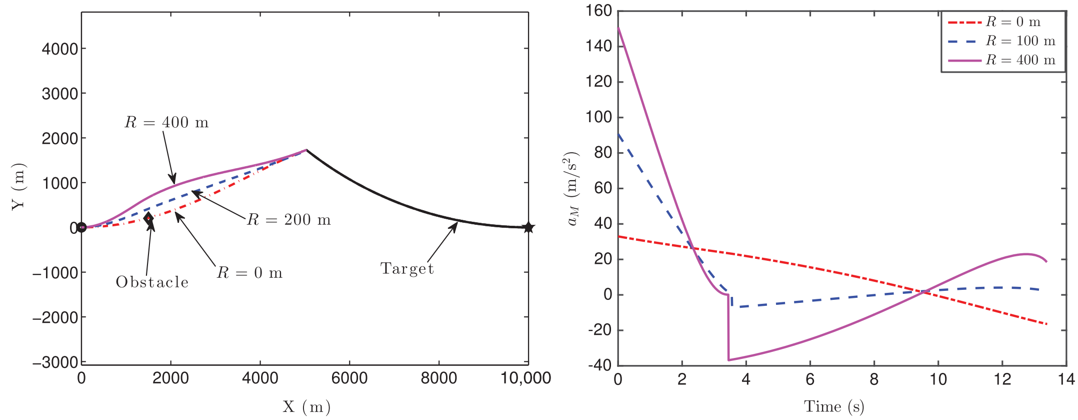

a) Trajectories of adversaries b) Missile lateral acceleration

Fig. 6 Interception at an impact angle of 60 deg with a target maneuver of 20 m/s^2 using nonlinear dynamics in the presence of a single obstacle.

Simulations were also performed with nonlinear kinematics, and the results are shown in Fig. 6. Results with the nonlinear simulation are similar to those with the linear simulation. The major change can be noticed in the missile lateral acceleration profile shown in Fig. 6b. The jump in missile lateral acceleration is due to changing the focus of the guidance command from obstacle avoidance to target interception with a desired impact angle; this is before the actual time to go corresponding to the obstacle becomes zero. The deviation in the missile lateral acceleration profile from its linear behavior can also be seen toward interception in Fig. 6b.

Remark 7: It is important to note here that the problem formulation for guidance derivation is based on small angle deviations for both the missile and target from the collision course. The proposed guidance scheme enables the missile to achieve its objective if the underlying assumptions are valid for the considered engagement scenario. However, if the actual engagement geometry is very far from the one assumed for guidance derivation, the proposed guidance scheme may not perform as expected. If the missile is launched in a direction with a high heading error or the target has a large heading error, then the performance of the guidance strategy degrades.

B. Two Obstacles

This subsection focuses on investigating the effect of the positions of obstacles and the different desired obstacle distances on the performance of the proposed guidance law. First, the engagement scenarios with two obstacles, located at the positions given by $(X_{1o}, Y_{1o}) = (1500, 200)$ m and $(X_{2o}, Y_{2o}) = (2500, 500)$ m, unless specified otherwise, are considered. Simulation parameters

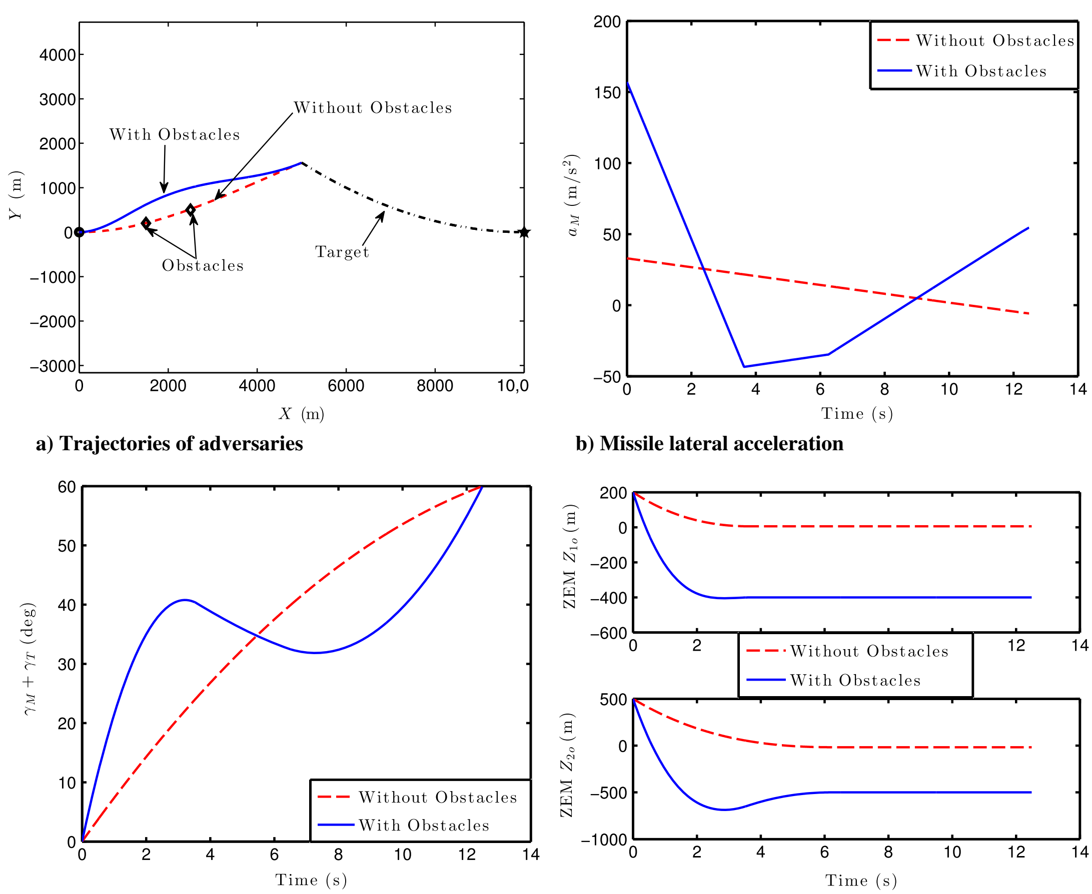

a) Trajectories of adversaries b) Missile lateral acceleration

c) Variation of relative course of missile and target d) Zero-effort miss with respect to obstacle

Fig. 7 Interception at an impact angle of 60 deg with a target maneuver of 20 m/s^2 using linear dynamics in the presence of two obstacles.

Table 2 Positions of obstacles

Engagements	Obstacle 1(X, Y)	Obstacle 2(X, Y)
Scenario 1	(1500, 800) m	(2500, 700) m
Scenario 2	(1500, 500) m	(2500, 1000) m
Scenario 3	(1500, 200) m	(2500, 1800) m

and initial conditions are assumed to be the same as those listed in Table 1. A desired impact angle and the desired distances from obstacles (R_1 and R_2) are considered to be 60 deg, 400 m, and 500 m, respectively. Simulation results with linear kinematics are shown in Fig. 7.

With the proposed guidance law, the missile is able to perform interception of the target at the desired impact angle, as shown in Fig. 7. Results for the scenario, where the missile focuses only on interception with a desired impact angle, are also plotted in Fig. 7 for the clear visualization of the effect of the proposed algorithm. It can be seen from Fig. 7a that the missile violates the boundary of both obstacles if it does not take into account obstacle avoidance. The profile of the missile lateral acceleration, as shown in Fig. 7b, is also piecewise linear with respect to time. Similar to the single-obstacle case, the slope of the missile's lateral acceleration profile changes twice due to the presence of the two obstacles. Lastly, Fig. 7d confirms that the desired minimum separation of the missile from both obstacles is maintained.

To investigate the effectiveness of the proposed guidance law, simulations are carried out for three different scenarios, listed in Table 2. The desired minimum distances from the obstacles and the desired impact angle are considered as $(R_1, R_2) = (400, 500)$ m and 0 deg, respectively. The results for this case are shown in Fig. 8. The missile is able to achieve its objectives in all the cases. From Fig. 8a, we see that the missile orients its trajectory from a single side of both obstacles for scenarios 2 and 3. But, the trajectory of the missile for scenario 1 is more interesting because it passes between both obstacles. This behavior is due to the optimization of the total control effort. For scenario 2, the missile does not need to perform an additional maneuver to avoid the second obstacle after it has passed the first obstacle. Similarly, for scenario 3, the missile does not require any extra effort for the first obstacle. However, for scenario 1, the missile has to perform maneuvers to avoid both obstacles as shown in Fig. 8b.

To understand the effect of the desired minimum distances from both obstacles, simulations are carried out with different desired distances from one obstacle while keeping the other fixed. The results with different distances from the first and second obstacles are plotted in Figs. 9 and 10, respectively. It can be observed from Fig. 9 that the missile has to apply a large maneuver to overcome the large required distance from the obstacle. As the obstacle radius increases, the missile also changes its course and passes along the other side. As shown in Fig. 10, the missile shows a similar behavior when the distance from the second obstacle is changed.

To observe the effect of the flight time, simulations are performed with different initial missile–target distances, and the results are plotted in Fig. 11. The performance for two obstacles is similar to that for the single-obstacle case. The distances from both obstacles are maintained, and the total control effort increases for the smaller flight time.

Simulation results with nonlinear kinematics are presented in Fig. 12, where trajectories for intercept angle guidance are also

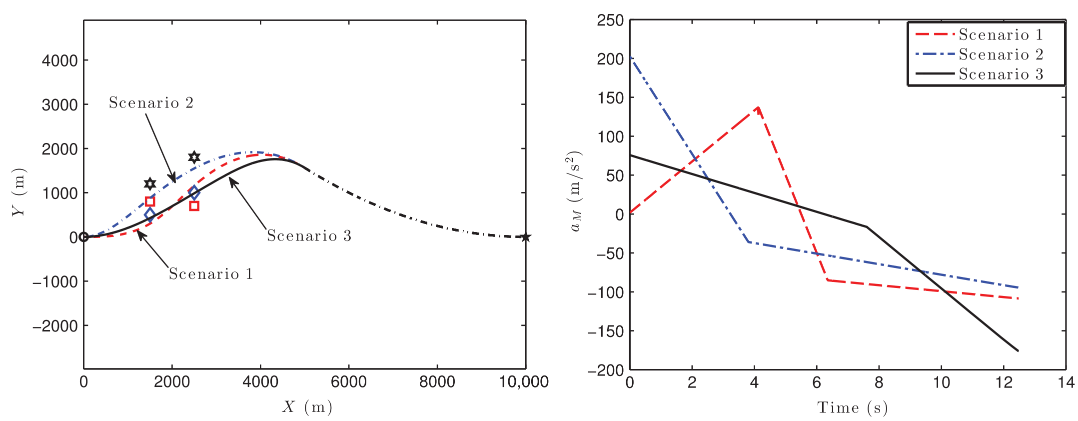

a) Trajectories of adversaries b) Missile lateral accelerations

Fig. 8 Performance of proposed guidance for different positions of obstacles with an impact angle of 0 deg.

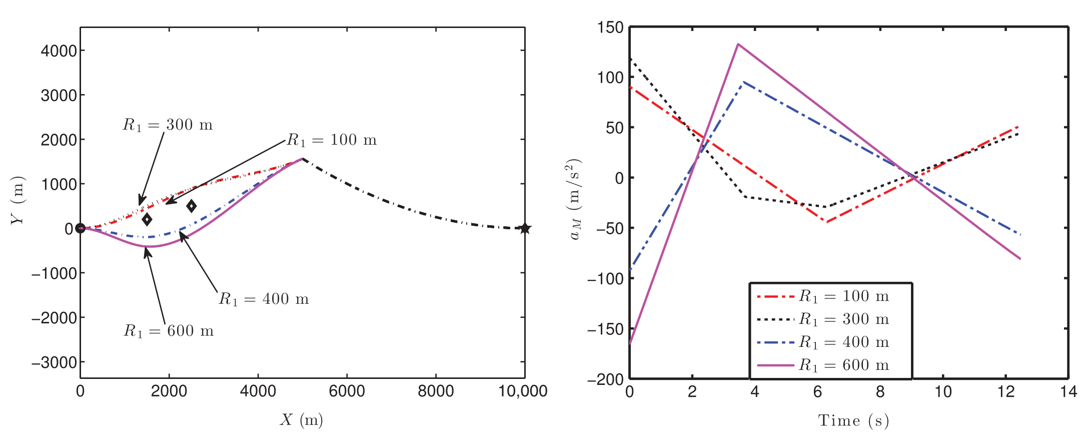

a) Trajectories of adversaries b) Missile lateral accelerations

Fig. 9 Performance of proposed guidance for different desired distances with respect to the first obstacle while that with the second obstacle is fixed to $R_2 = 400$ m.

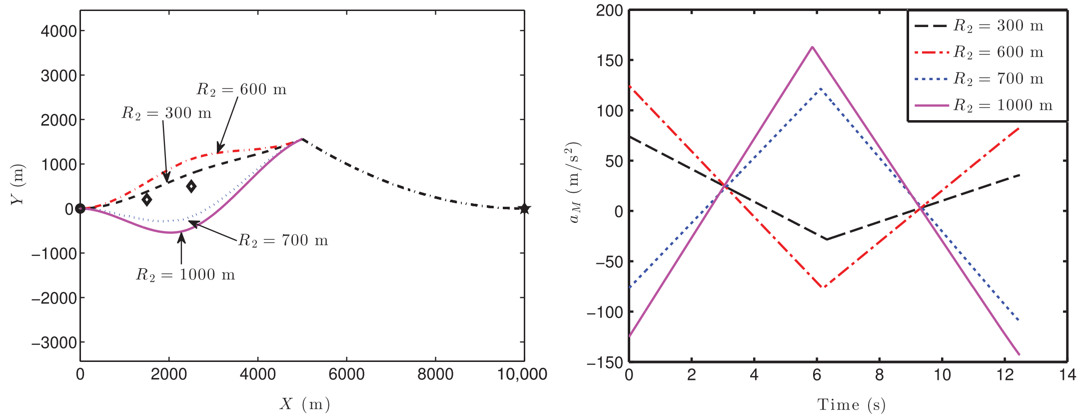

a) Trajectories of adversaries **b) Missile lateral accelerations**

Fig. 10 Performance of proposed guidance for different desired distances with respect to the second obstacle while that with the first obstacle is fixed to $R_1 = 100$ m.

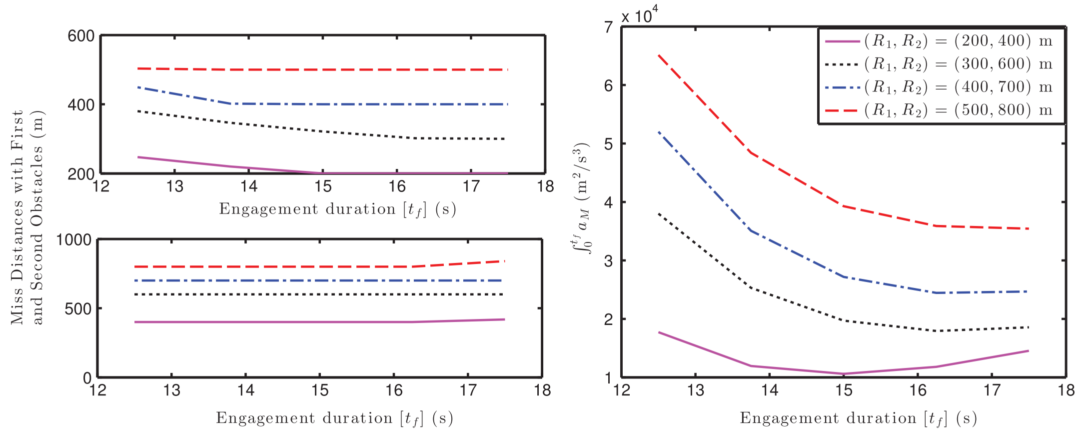

a) Miss distances with respect to obstacle **b) Total control efforts of missile**

Fig. 11 Performance of proposed guidance with respect to time of flight in the presence of two obstacles.

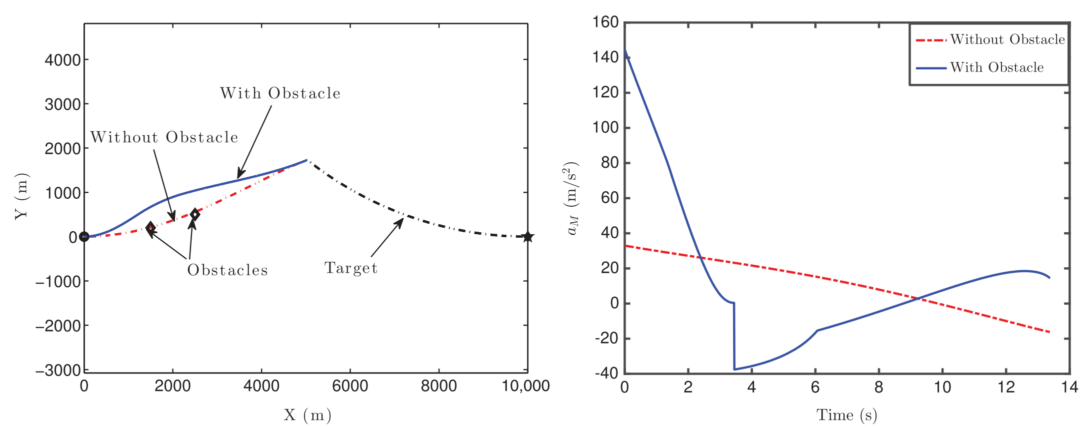

a) Trajectories of adversaries **b) Missile lateral acceleration**

Fig. 12 Interception at an impact angle of 60 deg with a target maneuver of 20 $\mathrm{m/s^2}$ using nonlinear dynamics in the presence of two obstacles.

shown. The behavior is similar to the single-obstacle case, as shown in Fig. 6. Due to the presence of two obstacles, two jumps can be noticed in the missile lateral acceleration profile, as shown in Fig. 12b.

VI. Conclusions

In this paper, an optimal control-based intercept angle guidance law was derived for a multiple-obstacle environment. The proposed guidance law not only achieves desired terminal constraints but also guarantees a minimum, prespecified separation from the obstacles along the trajectory.

The guidance command takes a form similar to that of augmented proportional navigation guidance with some bias terms. The bias terms correct for the impact angle error and generate maneuvers to avoid the obstacles.

An interesting feature of the derived guidance law is its generic nature. The term in the guidance command corresponding to obstacle avoidance has an intuitive structure, which highlights the contributions of each obstacle. Due to the simple structure, the proposed guidance law can be implemented for many obstacles, provided the solution of a finite-dimensional constrained optimization problem is computed. However, the computational burden increases for a large number of obstacles. Simulation results for one and two obstacles are presented to evaluate the effectiveness of the proposed guidance law for different positions of the obstacles, impact angles, and target maneuvers.

In the proposed guidance law, the obstacle detection and generation of required guidance commands are performed in a single step. This advantage may prove interesting for the practical implementation of the guidance law.

Although the derivation of the guidance law assumed linear kinematics and "close to collision course" trajectories, the simulation results on nonlinear kinematics and realistic planar trajectories indicated that the proposed guidance law worked and provided similar performance when these simplifying assumptions did not hold. How far the assumptions can be relaxed without deteriorating the expected performance will be part of future research efforts.

Appendix A: Existence of Lagrange Multipliers

The following result is Theorem 2.0 in Section 3.10 of [34].

Theorem 1: Let H be a Hilbert space and $\boldsymbol{y}_1, \boldsymbol{y}_2, \ldots, \boldsymbol{y}_N$ a set of linearly independent vectors in H. Among all vectors of H satisfying $(\boldsymbol{x}, \boldsymbol{y}_i) = c_i, \boldsymbol{i} = 1, \ldots, N$, where c_i are arbitrary scalars, the one that has the minimum norm is given by

$$\boldsymbol{x}_{\min} = \sum_{i=1}^{N} \beta_i \boldsymbol{y}_i, \qquad i = 1 \tag{A1}$$

where the coefficients β_i satisfy the linear system of equations

$$\sum_{i=1}^{N} (\boldsymbol{y}_i, \boldsymbol{y}_j)\beta_i = c_j, \qquad j = 1, \ldots, N \tag{A2}$$

In the paper, we use this result for the Hilbert space $H = L^2[t_0, t_f]$ with the inner product defined as

$$(f, g) = \int_0^{t_f} f(t) g(t)\, \mathrm{d}t \tag{A3}$$

Appendix B: Proof of Proposition 1

By using the Schur decomposition [35], the matrix inverse G^{-1} can be factorized as

$$G^{-1} = \begin{bmatrix} \boldsymbol{I} & G_{12_I} G_{2_I}^{-1} \\ 0 & \boldsymbol{I} \end{bmatrix} \begin{bmatrix} G_{1_I} - G_{12_I} G_{2_I}^{-1} G_{12_I}^T & 0 \\ 0 & G_{2_I} \end{bmatrix} \begin{bmatrix} \boldsymbol{I} & 0 \\ G_{2_I}^{-1} G_{12_I}^T & \boldsymbol{I} \end{bmatrix} \tag{B1}$$

By substituting Eq. (B1) in Eq. (23), we obtain

$$\begin{aligned} \boldsymbol{Z}_o^{d\star} &= \arg\min_{Z_o^d \in S} \begin{bmatrix} \boldsymbol{Z}_I \\ \boldsymbol{Z}_o - \boldsymbol{Z}_o^d \end{bmatrix}^T \begin{bmatrix} I & G_{12_I} G_{2_I}^{-1} \\ 0 & I \end{bmatrix} \begin{bmatrix} G_{1_I} - G_{12_I} G_{2_I}^{-1} G_{12_I}^T & 0 \\ 0 & G_{2_I} \end{bmatrix} \begin{bmatrix} I & 0 \\ G_{2_I}^{-1} G_{12_I}^T & I \end{bmatrix} \begin{bmatrix} \boldsymbol{Z}_I \\ \boldsymbol{Z}_o - \boldsymbol{Z}_o^d \end{bmatrix} \\ &= \arg\min_{Z_o^d \in S} \begin{bmatrix} \boldsymbol{Z}_I \\ G_{2_I}^{-1} G_{12_I}^T \boldsymbol{Z}_I + (\boldsymbol{Z}_o - \boldsymbol{Z}_o^d) \end{bmatrix}^T \begin{bmatrix} G_{1_I} - G_{12_I} G_{2_I}^{-1} G_{12_I}^T & 0 \\ 0 & G_{2_I} \end{bmatrix} \begin{bmatrix} \boldsymbol{Z}_I \\ G_{2_I}^{-1} G_{12_I}^T \boldsymbol{Z}_I + (\boldsymbol{Z}_o - \boldsymbol{Z}_o^d) \end{bmatrix} \\ &= \arg\min_{Z_o^d \in S} \boldsymbol{Z}_I^T \left(G_{1_I} - G_{12_I} G_{2_I}^{-1} G_{12_I}^T \right) \boldsymbol{Z}_I + \left[G_{2_I}^{-1} G_{12_I}^T \boldsymbol{Z}_I + (\boldsymbol{Z}_o - \boldsymbol{Z}_o^d) \right]^T G_{2_I} \left[G_{2_I}^{-1} G_{12_I}^T \boldsymbol{Z}_I + (\boldsymbol{Z}_o - \boldsymbol{Z}_o^d) \right] \\ &= \arg\min_{Z_o^d \in S} (\boldsymbol{Z}_o^d - \boldsymbol{Z}_o)^T G_{2_I} (\boldsymbol{Z}_o^d - \boldsymbol{Z}_o) - 2\boldsymbol{Z}_I^T G_{12_I} (\boldsymbol{Z}_o^d - \boldsymbol{Z}_o) + \boldsymbol{Z}_I^T \left(G_{1_I} - G_{12_I} G_{2_I}^{-1} G_{12_I}^T \right) \boldsymbol{Z}_I + \boldsymbol{Z}_I^T G_{12_I} G_{2_I}^{-1} G_{12_I}^T \boldsymbol{Z}_I \end{aligned} \tag{B2}$$

By decomposing $(\boldsymbol{Z}_o^d - \boldsymbol{Z}_o)$ as $(\boldsymbol{Z}_o^d - \boldsymbol{Z}_c) + (\boldsymbol{Z}_c - \boldsymbol{Z}_o)$ and using the definition of Z_c, Eq. (B2) can be reduced after some algebraic manipulations to

$$\begin{aligned} \boldsymbol{Z}_o^{d\star} &= \arg\min_{Z_o^d \in S} (\boldsymbol{Z}_o^d - \boldsymbol{Z}_c)^T G_{2_I} (\boldsymbol{Z}_o^d - \boldsymbol{Z}_c) - 2\boldsymbol{Z}_I^T G_{12_I} (\boldsymbol{Z}_c - \boldsymbol{Z}_o) \\ &\quad + (\boldsymbol{Z}_c - \boldsymbol{Z}_o)^T G_{2_I} (\boldsymbol{Z}_c - \boldsymbol{Z}_o) + \boldsymbol{Z}_I^T \left(G_{1_I} - G_{12_I} G_{2_I}^{-1} G_{12_I}^T \right) \boldsymbol{Z}_I \\ &\quad + \boldsymbol{Z}_I^T G_{12_I} G_{2_I}^{-1} G_{12_I}^T \boldsymbol{Z}_I \\ &= \arg\min_{Z_o^d \in S} \left(\boldsymbol{Z}_o^d - \boldsymbol{Z}_c \right)^T G_{2_I} \left(\boldsymbol{Z}_o^d - \boldsymbol{Z}_c \right) \\ &\quad + \boldsymbol{Z}_I^T \left(G_{1_I} - G_{12_I} G_{2_I}^{-1} G_{12_I}^T \right) \boldsymbol{Z}_I \end{aligned} \tag{B3}$$

Because the last term does not depend on Z_o^d, we obtain Eq. (25).

Appendix C: Proof of Proposition 2

Using $Z_o^{d\star}$ in Eq. (19), the Lagrange multipliers are

$$\begin{bmatrix} \boldsymbol{\lambda}_I \\ \boldsymbol{\lambda}_o \end{bmatrix} = \begin{bmatrix} G_{1_I} \boldsymbol{Z}_I + G_{12_I} (\boldsymbol{Z}_o - \boldsymbol{Z}_o^{d\star}) \\ G_{12_I}^T \boldsymbol{Z}_I + G_{2_I} (\boldsymbol{Z}_o - \boldsymbol{Z}_o^{d\star}) \end{bmatrix} \tag{C1}$$

On substituting for $(\boldsymbol{Z}_o - \boldsymbol{Z}_o^{d\star})$ from Eq. (28) in Eq. (C1) and performing some simplifications, we get

$$\begin{aligned} \begin{bmatrix} \boldsymbol{\lambda}_I \\ \boldsymbol{\lambda}_o \end{bmatrix} &= \begin{bmatrix} G_{1_I} \boldsymbol{Z}_I - G_{12_I} [G_{2_I}^{-1} (\Psi_{S,Q}(\boldsymbol{Z}_c) + G_{12_I}^T \boldsymbol{Z}_I)] \\ -\Psi_{S,G_{2_I}}(\boldsymbol{Z}_c) \end{bmatrix} \\ &= \begin{bmatrix} G_{1_I} - G_{12_I} G_{2_I}^{-1} G_{12_I}^T \\ 0 \end{bmatrix} \boldsymbol{Z}_I - \begin{bmatrix} G_{12_I} G_{2_I}^{-1} \\ I \end{bmatrix} \Psi_{S,G_{2_I}}(\boldsymbol{Z}_c) \end{aligned} \tag{C2}$$

Note that the matrix inverse of G can be written in the block matrices form as [35]

$$\begin{bmatrix} G_{1_I} & G_{12_I} \\ G_{12_I}^T & G_{2_I} \end{bmatrix} = \begin{bmatrix} (G_1 - G_{12}G_2^{-1}G_{12}^T)^{-1} & -G_1^{-1}G_{12}(G_2 - G_{12}^T G_1^{-1} G_{12})^{-1} \\ -(G_2 - G_{12}^T G_1^{-1} G_{12})^{-1} G_{12}^T G_1^{-1} & (G_2 - G_{12}^T G_1^{-1} G_{12})^{-1} \end{bmatrix} \tag{C3}$$

provided the matrices $G_1, G_2, G_1 - G_{12}G_2^{-1}G_{12}^T$ and $G_2 - G_{12}^T G_1^{-1} G_{12}$ are invertible. Also, it is known from the Woodbury matrix identity [36] that

$$\begin{aligned}(G_1 - G_{12}G_2^{-1}G_{12}^T)^{-1} \\ = G_1^{-1} + G_1^{-1}G_{12}(G_2 - G_{12}^T G_1^{-1} G_{12})^{-1} G_{12}^T G_1^{-1}\end{aligned} \tag{C4}$$

subjected to the condition that the inverse of the matrices in Eq. (C4) exists.

Now, simplifying $G_{1_I} - G_{12_I} G_{2_I}^{-1} G_{12_I}^T$ after substituting for the matrices G_{1_I}, G_{12_I}, and G_{2_I} from Eq. (C3), and using the Woodbury matrix identity [Eq. (C4)], we obtain

$$\begin{aligned} &G_{1_I} - G_{12_I} G_{2_I}^{-1} G_{12_I}^T \\ &= (G_1 - G_{12}G_2^{-1}G_{12}^T)^{-1} - G_1^{-1}G_{12}(G_2 - G_{12}^T G_1^{-1} G_{12})^{-1} G_{12}^T G_1^{-1} \\ &= G_1^{-1} \end{aligned} \tag{C5}$$

By using Eq. (C5), the expressions for the Lagrange multipliers [Eq. (C2)] reduce to

$$\begin{aligned}\begin{bmatrix} \boldsymbol{\lambda}_I \\ \boldsymbol{\lambda}_o \end{bmatrix} &= \begin{bmatrix} G_1^{-1}\mathbf{Z}_I - G_{12_I} G_{2_I}^{-1} \Psi_{S,G_{2_I}}(\mathbf{Z}_c) \\ -\Psi_{S,G_{2_I}}(\mathbf{Z}_c) \end{bmatrix} \\ &= \begin{bmatrix} G_1^{-1}\mathbf{Z}_I + G_1^{-1} G_{12} \Psi_{S,G_{2_I}}(\mathbf{Z}_c) \\ -\Psi_{S,G_{2_I}}(\mathbf{Z}_c) \end{bmatrix}\end{aligned} \tag{C6}$$

which is the same as those given in Eq. (29).

Appendix D: Generalized Dead-Zone Function

The generalized dead-zone function $\Psi_{S,Q}(\cdot)$ [37], associated with subset $S \in \mathbb{R}^N$ and positive definite matrix $Q \in \mathbb{R}^{N\times N}$, is defined as the mapping $\Psi_{S,Q}:\mathbb{R}^N \to \mathbb{R}^N$ such that

$$\Psi_{S,Q}(\mathbf{Z}) = Q(\mathbf{z}^\star - \mathbf{Z}) \tag{D1}$$

where $\mathbf{z} = [z_{1o}^d \ \dots \ z_{io}^d \ \dots \ z_{2o}^d]^T$, $\mathbf{Z} = [Z_{1c} \ \dots \ Z_{ic} \ \dots \ Z_{Nc}]^T$, and the minimizer $\mathbf{z}^\star \in \mathbb{R}^N$ is given by

$$\mathbf{z}^\star = \arg\min_{z\in S} (\mathbf{z} - \mathbf{Z})^T Q (\mathbf{z} - \mathbf{Z}) \tag{D2}$$

Due to the positive definiteness of the matrix Q, the solution of the problem specified in Eq. (D2) always exists. In cases where the subset $\boldsymbol{S}$ is convex, the minimum value $\mathbf{z}^\star$ is unique and can be used to define the dead-zone function. Unfortunately, the subset $\boldsymbol{S}$ in our problem is not even connected, and there may exist many solutions. One of these possible solutions is used to define the dead-zone function in Eq. (D1).

It is important to note that, if the vector $\mathbf{Z}$ belongs to the subset $\boldsymbol{S}$, then $\mathbf{z}^\star = \mathbf{Z}$. As a result, $\Psi_{S,Q}(\mathbf{Z}) = 0$, which makes the subset S a dead zone, and it justifies the name of function $\Psi_{S,Q}(\cdot)$.

Appendix E: One-Dimensional Generalized Dead-Zone Function

In the guidance derivation for an engagement scenario with one obstacle, the one-dimensional generalized dead-zone function with a nonconnected dead zone of the form

$$\boldsymbol{S}_{R_1} = \left\{ Z_{1o}^d \in \mathbb{R} \,|\, |Z_{1o}^d| > R_1 \right\} \tag{E1}$$

is used. To obtain the optimum value of the problem given in Eq. (D2) for one-obstacle cases, consider an optimization problem with the cost function as

$$J_{\text{opt}}(Z_{1o}^d) = (Z_{1o}^d - Z_{1c})^T Q (Z_{1o}^d - Z_{1c}) \tag{E2}$$

On minimizing Eq. (E2) while satisfying the constraints $|Z_{1o}^d| > R_1$, we obtain

$$Z_{1o}^{d\star} = \begin{cases} Z_{1c} & |Z_{1c}| \ge R_1 \\ R_1 \operatorname{sign}(Z_{1c}) & |Z_{1c}| < R_1 \end{cases} \tag{E3}$$

From Eq. (E3), it can be shown that

$$Z_{1o}^{d\star} - Z_{1c} = -\psi_{R_1}(Z_{1c}) \tag{E4}$$

where the function $\psi_R(p)$, represented graphically in Fig. E1, is defined as [38]

$$\psi_R(p) = \begin{cases} 0 & |p| \ge R \\ p - R & 0 \le p \le R \\ p + R & -R < p < 0 \end{cases} \tag{E5}$$

On using the definition of the dead-zone function [Eq. (D1)] and Eq. (E4), we obtain

$$\Psi_{S,Q}(Z_{1c}) = Q(Z_{1o}^{d\star} - Z_{1c}) = -Q\psi_{R_1}(Z_{1c}) \tag{E6}$$

Appendix F: Two-Dimensional Generalized Dead-Zone Function

In the derivation of the proposed guidance for two obstacles, a two-dimensional generalized dead-zone function with a nonconnected dead zone of the form

$$\boldsymbol{S}_{R_1,R_2} = \left\{ [Z_{1o}^d \quad Z_{2o}^d]^T \in \mathbb{R}^2 \,|\, |Z_{1o}^d| > R_1, |Z_{2o}^d| > R_2 \right\} \tag{F1}$$

is used. Because the set $\boldsymbol{S}_{R_1,R_2}$ consists of four convex sets, the optimal solution to the constrained optimization problem can be obtained numerically by using iterative methods. This method will find a minimum solution in every convex set, and the one among these solutions can be chosen as the optimal solution. Because this

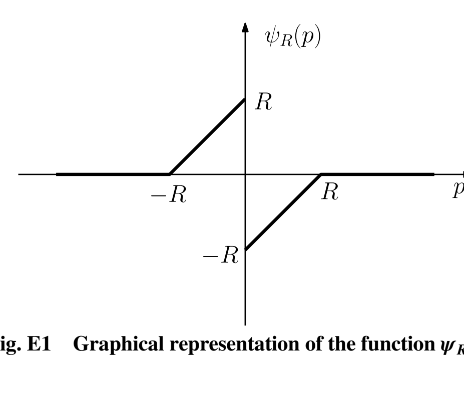

Fig. E1 Graphical representation of the function $\psi_R(p)$.

function has a direct use in the guidance law, this appendix presents an efficient way to compute the optimal solution.

To obtain the optimum value of the problem given in Eq. (D2) for a two-obstacle engagement scenario, consider an optimization problem with the cost function as

$$J_{\mathrm{opt}}(Z_{1o}^d, Z_{2o}^d) = \begin{bmatrix} Z_{1o}^d - Z_{1c} \\ Z_{2o}^d - Z_{2c} \end{bmatrix}^T \begin{bmatrix} q_1 & -q_3 \\ -q_3 & q_2 \end{bmatrix} \begin{bmatrix} Z_{1o}^d - Z_{1c} \\ Z_{2o}^d - Z_{2c} \end{bmatrix} \tag{F2}$$

subjected to the conditions $|Z_{1o}^d| \geq R_1$ and $|Z_{2o}^d| \geq R_2$. Note that $q_1, q_2 > 0$, $q_1 q_2 > q_3^2$, and q_3 is assumed to be positive for the time instant. Following the technique in [37], let us first optimize with respect to Z_{2o}^d while keeping Z_{1o}^d arbitrary; that is, solve the problem

$$\min_{|Z_{2o}^d| \geq R_2} J_{\mathrm{opt}}(Z_{1o}^d, Z_{2o}^d)$$

The solution to this problem is

$$Z_{2o}^{d\star}(Z_{1o}^d) = \begin{cases} Z_{2c} + \dfrac{q_3}{q_2}(Z_{1o}^d - Z_{1c}), & \left| Z_{2c} + \dfrac{q_3}{q_2}(Z_{1o}^d - Z_{1c}) \right| \geq R_2 \\ R_2 \mathrm{sign}\left(Z_{2c} + \dfrac{q_3}{q_2}(Z_{1o}^d - Z_{1c}) \right), & \text{otherwise} \end{cases} \tag{F3}$$

On defining the notations

$$\bar{Z}_{1o} = Z_{1c} - \frac{q_2}{q_3} Z_{2c}, \quad \bar{Z}_{1+} = Z_{1c} + \frac{q_2}{q_3}(R_2 - Z_{2c}), \quad \bar{Z}_{1-} = Z_{1c} - \frac{q_2}{q_3}(R_2 + Z_{2c}) \tag{F4}$$

we can rewrite the solution of the preceding problem as

$$Z_{2o}^{d\star}(Z_{1o}^d) = \begin{cases} Z_{2c} + \dfrac{q_3}{q_2}(Z_{1o}^d - Z_{1c}), & Z_{1o}^d \leq \bar{Z}_{1-} \text{ or } Z_{1o}^d \geq \bar{Z}_{1+} \\ R_2, & \bar{Z}_{1-} \leq Z_{1o}^d \leq \bar{Z}_{1o} \\ -R_2, & \bar{Z}_{1o} \leq Z_{1o}^d \leq \bar{Z}_{1+} \end{cases} \tag{F5}$$

Now, the expression for $J_{\mathrm{opt}}(Z_{1o}^d, Z_{2o}^{d\star})$ becomes

$$J_{\mathrm{opt}}(Z_{1o}^d) = J_{\mathrm{opt}}\left\{ Z_{1o}^d, Z_{2o}^{d\star}(Z_{1o}^d) \right\} = \begin{cases} \dfrac{q_1 q_2 - q_3^2}{q_2}(Z_{1o}^d - Z_{1c})^2, & Z_{1o}^d \leq \bar{Z}_{1-} \text{ or } Z_1^d \geq \bar{Z}_{1+} \\ (Z_{1o}^d - Z_{1-})^2 + \dfrac{q_1 q_2 - q_3^2}{q_2}(R_2 - Z_{2c})^2, & \bar{Z}_{1-} \leq Z_1^d \leq \bar{Z}_{1o} \\ (Z_{1o}^d - Z_{1+})^2 + \dfrac{q_1 q_3 - q_3^2}{q_2}(R_2 + Z_{2c})^2, & \bar{Z}_{1o} \leq Z_1^d \leq \bar{Z}_{1+} \end{cases} \tag{F6}$$

where

$$Z_{1+} = Z_{1c} + \frac{q_3}{q_1}(R_2 - Z_{2c}), \quad Z_{1-} = Z_{1c} - \frac{q_3}{q_1}(R_2 + Z_{2c}) \tag{F7}$$

To obtain the minimum of function $J_{\mathrm{opt}}(Z_{1o}^d)$ satisfying $|Z_{1o}^d| \geq R_1$, the following points can be considered:

$$Z_{1_{1,2}}^d = \pm R_1, \quad Z_{1_{3,4}}^d = Z_{1\pm}, \quad Z_{1_{5,6}}^d = Z_{1c,o}, \quad Z_{1_{7,8}}^d = \bar{Z}_{1\pm} \tag{F8}$$

Note that $Z_{1o_{1,2}}^d$ always satisfies $|Z_{1o}| \geq R_1$, but the other points need to be checked for this condition. The optimum value of $J_{\mathrm{opt}}(Z_{1o}^d)$ can be obtained on the point $Z_{1o}^{d\star}$ such that it satisfies

$$J_{\mathrm{opt}}(Z_{1o}^{d\star}) = \min_{|Z_{1o}^d| \geq R_1} J_{\mathrm{opt}}(Z_{1o}^d) \tag{F9}$$

and the minimum of $J_{\mathrm{opt}}(Z_{1o}^d, Z_{2o}^d)$ will be achieved at the point $[Z_{1o}^{d\star}, Z_{2o}^{d\star}(Z_{1o}^{d\star})]$.

For the cases of $q_3 < 0$, we have $\bar{Z}_{1-} > \bar{Z}_{1+}$; and the expression for $Z_{2o}^{d\star}$ will be changed to

$$Z_{2o}^{d\star}(Z_{1o}^d) = \begin{cases} Z_{2c} + \dfrac{q_3}{q_2}(Z_{1o}^d - Z_{1c}), & Z_{1o}^d \leq \bar{Z}_{1+} \text{ or } Z_{1o}^d \geq \bar{Z}_{1-} \\ R_2, & \bar{Z}_{1+} \leq Z_{1o}^d \leq \bar{Z}_{1o} \\ -R_2, & \bar{Z}_{1o} \leq Z_{1o}^d \leq \bar{Z}_{1-} \end{cases} \tag{F10}$$

Consequently, in the formula for $J_{\mathrm{opt}}(Z_{1o}^d)$, the terms $\bar{Z}_{1-}$ and $\bar{Z}_{1+}$ change their places without affecting the rest of the expressions.

After computing the optimal solution of the optimization problem [Eq. (F2)], the dead-zone function in this case is given by

$$\Psi_{S,Q} \begin{bmatrix} Z_{1c} \\ Z_{2c} \end{bmatrix} = Q \begin{bmatrix} Z_{1o}^{d\star} - Z_{1c} \\ Z_{2o}^{d\star} - Z_{2c} \end{bmatrix} \tag{F11}$$

Acknowledgment

This research was partially supported by the Technion Autonomous Systems Program.

References

[1] Kim, M., and Grider, K., "Terminal Guidance for Impact Attitude Angle Constrained Flight Trajectories," *IEEE Transactions on Aerospace and Electronic Systems*, Vol. AES-9, No. 6, 1973, pp. 852–859. doi:10.1109/TAES.1973.309659

[2] Ryoo, C. K., Cho, H., and Tahk, M. J., "Time-to-Go Weighted Optimal Guidance with Impact Angle Constraints," *IEEE Transactions on Control Systems Technology*, Vol. 14, No. 3, 2006, pp. 483–492. doi:10.1109/TCST.2006.872525

[3] Shaferman, V., and Shima, T., "Linear Quadratic Guidance Laws for Imposing a Terminal Intercept Angle," *Journal of Guidance, Control, and Dynamics*, Vol. 31, No. 5, 2008, pp. 1400–1412. doi:10.2514/1.32836

[4] Lu, P., Doman, D., and Schierman, J., "Adaptive Terminal Guidance for Hypervelocity Impact in Specified Direction," *Journal of Guidance, Control, and Dynamics*, Vol. 29, No. 2, 2006, pp. 269–278. doi:10.2514/1.14367

[5] Liu, X., Shen, Z., and Lu, P., "Closed-Loop Optimization of Guidance Gain for Constrained Impact," *Journal of Guidance, Control, and Dynamics*, Vol. 40, No. 2, 2017, pp. 453–460. doi:10.2514/1.G000323

[6] Kim, B., Lee, J., and Han, H., "Biased PNG Law for Impact with Angular Constraint," *IEEE Transactions on Aerospace and Electronic Systems*, Vol. 34, No. 1, 1998, pp. 277–288. doi:10.1109/7.640285

[7] Ratnoo, A., "Analysis of Two-Stage Proportional Navigation with Heading Constrains," *Journal of Guidance, Control, and Dynamics*, Vol. 39, No. 1, 2016, pp. 156–164. doi:10.2514/1.G001262

[8] Manchester, I. R., and Savkin, A. V., "Circular-Navigation-Guidance Law for Precision Missile/Target Engagements," *Journal of Guidance, Control, and Dynamics*, Vol. 29, No. 2, 2006, pp. 314–320. doi:10.2514/1.13275

[9] Tsalik, R., and Shima, T., "Inscribed Angle Guidance," *Journal of Guidance, Control, and Dynamics*, Vol. 38, No. 1, 2015, pp. 30–40. doi:10.2514/1.G000468

[10] Tsalik, R., and Shima, T., “Optimal Guidance Around Circular Trajectories for Impact-Angle Interception,” *Journal of Guidance, Control, and Dynamics*, Vol. 39, No. 6, 2016, pp. 1278–1291. doi:10.2514/1.G001759

[11] Kumar, S. R., Tsalik, R., and Shima, T., “Nonlinear Robust Inscribed Angle Guidance for Stationary Targets,” *Journal of Guidance, Control, and Dynamics*, Vol. 40, No. 7, 2017, pp. 1815–1823. doi:10.2514/1.G002461

[12] Shima, T., “Intercept-Angle Guidance,” *Journal of Guidance, Control, and Dynamics*, Vol. 34, No. 2, 2011, pp. 484–492. doi:10.2514/1.51026

[13] Kumar, S. R., Rao, S., and Ghose, D., “Sliding-Mode Guidance and Control for All-Aspect Interceptor with Terminal Angle Constraints,” *Journal of Guidance, Control, and Dynamics*, Vol. 35, No. 4, 2012, pp. 1230–1246. doi:10.2514/1.55242

[14] Kumar, S. R., Rao, S., and Ghose, D., “Nonsingular Terminal Sliding Mode Guidance with Impact Angle Constraints,” *Journal of Guidance, Control, and Dynamics*, Vol. 37, No. 4, 2014, pp. 1114–1130. doi:10.2514/1.62737

[15] Lee, C. H., Kim, T. H., and Tahk, M. J., “Design of Impact Angle Control Guidance Laws via High-Performance Sliding Mode Control,” *Journal of Aerospace Engineering*, Vol. 227, No. 2, 2013, pp. 235–253. doi:10.1177/0954410011433732

[16] Tchuiev, V., and Shima, T., “Intercept Angle Guidance in an Obstacle-Rich Environment,” *Journal of Guidance, Control, and Dynamics*, Vol. 40, No. 6, 2017, pp. 1507–1518. doi:10.2514/1.G002355

[17] Karaman, S., and Frazzoli, E., “Sampling-Based Algorithms for Optimal Motion Planning,” *International Journal of Robotics Research*, Vol. 30, No. 7, 2011, pp. 846–894. doi:10.1177/0278364911406761

[18] Kochenderfer, M. J., Holland, J. E., and Chryssanthacopoulos, J. P., “Next Generation Airborne Collision Avoidance System,” *Lincoln Laboratory Journal*, Vol. 19, No. 1, 2012, pp. 17–33.

[19] Gottlieb, Y., and Shima, T., “UAVs Task and Motion Planning in the Presence of Obstacles and Prioritized Targets,” *Sensors*, Vol. 15, No. 2, 2015, pp. 29734–29764. doi:10.3390/s151129734

[20] Ferbach, P., “A Method of Progressive Constraints for Nonholonomic Motion Planning,” *Proceedings of the IEEE Conference on Robotics and Automation*, Vol. 4, IEEE Publ., Piscataway, NJ, 1996, pp. 2949–2955. doi:10.1109/70.660867

[21] Pettersson, P. O., and Doherty, P., “Probabilistic Roadmap Based Path Planning for an Autonomous Unmanned Helicopter,” *Journal of Intelligent & Fuzzy Systems*, Vol. 17, No. 4, 2006, pp. 395–405.

[22] Han, S. C., Bang, H., and Yoo, C. S., “Proportional Navigation-Based Collision Avoidance for UAVs,” *International Journal of Control, Automation and Systems*, Vol. 7, No. 4, 2009, pp. 553–565. doi:10.1007/s12555-009-0407-1

[23] Chakravarthy, A., and Ghose, D., “Obstacle Avoidance in a Dynamic Environment: A Collision Cone Approach,” *IEEE Transactions on Systems, Man, and Cybernetics, Part A: Systems and Humans*, Vol. 28, No. 5, 1998, pp. 562–574. doi:10.1109/3468.709600

[24] Chakravarthy, A., and Ghose, D., “Generalization of the Collision Cone Approach for Motion Safety in 3-D Environments,” *Autonomous Robots*, Vol. 32, No. 3, 2012, pp. 243–266. doi:10.1007/s10514-011-9270-z

[25] Jenie, Y. I., Kampen, E. J. V., Visser, C. C. D., Ellerbroek, J., and Hoekstra, J. M., “Selective Velocity Obstacle Method for Deconflicting Maneuvers Applied to Unmanned Aerial Vehicles,” *Journal of Guidance, Control, and Dynamics*, Vol. 38, No. 6, 2015, pp. 1140–1146. doi:10.2514/1.G000737

[26] Watanabe, Y., Calise, A. J., Johnson, E. N., and Evers, J. H., “Minimum-Effort Guidance for Vision-Based Collision Avoidance,” *AIAA Atmospheric Flight Mechanics Conference and Exhibit*, AIAA Paper 2006-6641, 2006, pp. 21–24. doi:10.2514/6.2006-6641

[27] Khatib, O., “Real-Time Obstacle Avoidance for Manipulators and Mobile Robots,” *International Journal of Robotics Research*, Vol. 5, No. 1, 1986, pp. 90–98. doi:10.1177/027836498600500106

[28] Paul, T., Krogstad, T. R., and Gravdahl, J. T., “Modelling of UAV Formation Flight Using 3D Potential Field,” *Simulation Modelling Practice and Theory*, Vol. 16, No. 9, 2008, pp. 1453–1462. doi:10.1016/j.simpat.2008.08.005

[29] Rimon, E., and Koditschek, D. E., “Exact Robot Navigation using Artificial Potential Functions,” *IEEE Transactions on Robotics and Automation*, Vol. 8, No. 5, 1992, pp. 501–518. doi:10.1109/70.163777

[30] Zhao, J., and Zhou, R., “Obstacle Avoidance for Multi-Missile Network via Distributed Coordination Algorithm,” *Chinese Journal of Aeronautics*, Vol. 29, No. 2, 2016, pp. 441–447. doi:10.1016/j.cja.2016.01.011

[31] Bryson, A. E., and Ho, Y. C., *Applied Optimal Control: Optimization, Estimation and Control*, Hemisphere, New York, 1975, pp. 148–176.

[32] Gutman, S., *Applied Min-Max Approach to Missile Guidance and Control*, Vol. 209, AIAA, New York, 2005, pp. 183–190, Chap. 7.

[33] Weiss, M., and Shima, T., “Linear Quadratic Optimal Guidance with Obstacle Avoidance,” *Proceedings of the International Conference on the Science of Electrical Engineering (ICSEE)*, IEEE Israel, Tel Aviv, Israel, Nov. 2016, pp. 1–13.

[34] Luenberger, D. G., *Optimization by Vector Space Methods*, Wiley, New York, 1969, pp. 65–66.

[35] Horn, R. A., and Johnson, C. R., *Matrix Analysis*, 1st ed., Cambridge Univ. Press, New York, 1990, pp. 425–516.

[36] Woodbury, M. A., “Inverting Modified Matrices,” Statistical Research Group, Princeton Univ. Memorandum Rept. 42, Princeton, NJ, 1950.

[37] Weiss, M., Shima, T., Castaneda, D., and Rusnak, I., “Combined and Cooperative Minimum Effort Guidance Algorithms in an Active Aircraft Defense Scenario,” *Journal of Guidance, Control, and Dynamics*, Vol. 40, No. 5, 2017, pp. 1241–1254. doi:10.2514/1.G002315

[38] Weiss, M., and Shima, T., “Minimum Effort Pursuit/Evasion Guidance with Specified Miss Distance,” *Journal of Guidance, Control, and Dynamics*, Vol. 39, No. 5, 2016, pp. 1069–1079. doi:10.2514/1.G001623